Journal of Medicinal Chemistry

Article

Discovery of N-((3R,4R)-4-fluoro-1-(6-((3-methoxy-1-methyl-1H-pyrazol-4-yl)amino)-9-methyl-9H-purin-2-yl)pyrrolidine-3-yl)acrylamide (PF-06747775) Through Structure-Based Drug Design; A High Affinity Irreversible Inhibitor Targeting Oncogenic EGFR Mutants With Selectivity Over Wild-Type EGFR.

Simon Planken, Douglas Carl Behenna, Sajiv K Nair, Theodore Otto Johnson, Asako Nagata, Chau Almaden, Simon Bailey, T. Eric Ballard, Louise Bernier, Hengmiao Cheng, Sujin Cho-Schultz, Deepak Dalvie, Judith G. Deal, Dac M Dinh, Martin P. Edwards, Rose Ann Ferre, Ketan S Gajiwala, Michelle D. Hemkens, Robert S Kania, John C. Kath, Jean Matthews, Brion W. Murray, Sherry Niessen, Suvi T M Orr, Mason Pairish, Neal W Sach, Hong Shen, Manli Shi, James Solowiej, Khanh Tran, Elaine Tseng, Paolo Vicini, Yuli Wang, Scott L. Weinrich, Ru Zhou, Michael Zientek, Longqing Liu, Yiqin Luo, Shuibo Xin, Chengyi Zhang, and Jennifer Anne Lafontaine

J. Med. Chem., **Just Accepted Manuscript** • DOI: 10.1021/acs.jmedchem.6b01894 • Publication Date (Web): 13 Mar 2017

Just Accepted

ACS Publications

Journal of Medicinal Chemistry is published by the American Chemical Society. 1155 Sixteenth Street N.W., Washington, DC 20036

	Tseng, Elaine; pfizer PGRD, PDM Vicini, Paolo; pfizer PGRD, Medicinal Sciences Wang, Yuli; Pfizer Global Research & Development, Oncology research unit Weinrich, Scott; Pfizer Global Research & Development, Oncology Research Unit Zhou, Ru; pfizer PGRD, Medicinal Sciences Zientek, Michael; Takeda Pharmaceuticals U.S.A., Inc., Liu, Longqing; WuXi AppTec Luo, Yiqin; WuXi AppTec Xin, Shuibo; WuXi App Tec Co., Shanghai, China, Zhang, Chengyi; WuXi AppTec Lafontaine, Jennifer; Pfizer Global Research and Development, Medicinal Chemistry

Discovery of *N*-((3*R*,4*R*)-4-fluoro-1-(6-((3-methoxy-1-methyl-1*H*-pyrazol-4-yl)amino)-9-methyl-9*H*-purin-2-yl)pyrrolidine-3-yl)acrylamide (PF-06747775) Through Structure-Based Drug Design; A High Affinity Irreversible Inhibitor Targeting Oncogenic EGFR Mutants With Selectivity Over Wild-Type EGFR.

Simon Planken*[†], Douglas C. Behenna*[†], Sajiv K. Nair[†], Theodore O. Johnson[†], Asako Nagata[†], Chau Almaden[‡], Simon Bailey[†], T. Eric Ballard[§], Louise Bernier[†], Hengmiao Cheng[†], Sujin Cho-Schultz[†], Deepak Dalvie[§], Judith G. Deal[†], Dac M. Dinh[‡], Martin P. Edwards[†], Rose Ann Ferre[†], Ketan S. Gajiwala[†], Michelle Hemkens[¥], Robert S. Kania[†], John C. Kath[†], Jean Matthews[†], Brion W. Murray[‡], Sherry Niessen[†], Suvi T. M. Orr[†], Mason Pairish[†], Neal W. Sach[†], Hong Shen[†], Manli Shi[‡], James Solowiej[‡], Khanh Tran[†], Elaine Tseng[§], Paolo Vicini[§], Yuli Wang[‡], Scott L. Weinrich[‡], Ru Zhou[†], Michael Zientek[§], Longqing Liu[Ɣ], Yiqin Luo[Ɣ], Shuibo Xin[Ɣ], Chengyi Zhang[Ɣ] and Jennifer Lafontaine[†].

Departments of [†]Worldwide Medicinal Chemistry, [§]Pharmacokinetics, Dynamics and Metabolism, [‡]Oncology Research Unit, [¥]Drug Safety, La Jolla Laboratories, Pfizer Worldwide Research and Development, 10770 Science Center Drive, San Diego, CA, 92121, United States. [Ɣ]Wuxi AppTec, 288 Fute Zhong Road, Waigaoqiao Free Trade Zone, Shanghai 200131, China.

Abstract: Mutant epidermal growth factor receptor (EGFR) is a major driver of non-small cell lung cancer (NSCLC). Marketed first generation inhibitors, such as erlotinib, effect a transient beneficial response in EGFR-mutant NSCLC patients before resistance mechanisms render these inhibitors ineffective. Secondary oncogenic EGFR mutations account for approximately 50% of relapses, the most common being the gatekeeper T790M substitution that renders existing therapies ineffective. The discovery of **PF-06459988 (1)**, an irreversible pyrrolopyrimidine inhibitor of EGFR T790M mutants was recently disclosed[1]. Herein, we describe our continued

efforts to achieve potency across EGFR oncogenic mutations and improved kinome selectivity, resulting in the discovery of clinical candidate **PF-06747775 (21)**, which provides potent EGFR activity against the four common mutants (exon 19 deletion (Del), L858R, and double mutants T790M/L858R and T790M/Del), selectivity over wild-type EGFR, and desirable ADME properties. Compound **21** is currently being evaluated in Phase-I clinical trials of mutant EGFR driven NSCLC.

Introduction:

Activating mutations in the Epidermal Growth Factor Receptor (EGFR) are one of the major drivers of non-small cell lung cancer (NSCLC)[2]. While reversible first generation EGFR inhibitors are initially an effective treatment, it is well documented that a drug resistant gatekeeper T790M mutation accounts for ~50% of disease progression in patients treated with first generation agents[2a, 3]. Irreversible second generation EGFR inhibitors, which covalently modify C797 in the ATP binding site of EGFR, are more potent against the T790M mutants[4]. These agents, however, are dose limited by their exceptional potency against wild-type (WT) EGFR, which drives mechanism-based toxicity[5]. Efforts to overcome this limitation led to the emergence of irreversible third generation EGFR inhibitors that provide effective potency against both drug resistant T790M mutants and the original activating mutants while sparing activity against WT EGFR[6].

The recently disclosed third generation EGFR inhibitor **PF-06459988** (compound **1**, Figure **1**) was discovered by *de novo* structure-based drug design with a strategic focus on improving inhibitor potency by increasing reversible binding affinity[1]. Implementation of this strategy enabled the intrinsic reactivity of the inhibitor's warhead functionality to be minimized in

parallel as a means to reduce the probability of any safety risks associated with an irreversible inhibitor mode of action[7]. Compound **1** provided low nM biochemical and cellular potency against both EGFR T790M resistant mutants (T790M/L858R and T790M/Del), excellent selectivity for the drug resistant mutants over WT EGFR and *in vitro* and *in vivo* ADME characteristics well suited for *in vivo* efficacy studies.

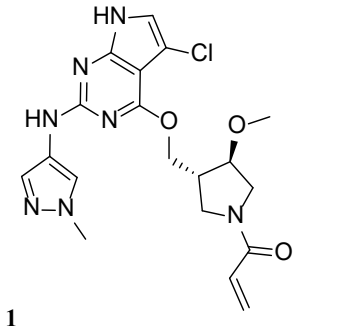

1
EGFR L858R_T790M IC_{50} 13 nM
EGFR Del_T790M IC_{50} 7 nM
EGFR L858R IC_{50} 21 nM
EGFR Del IC_{50} 140 nM
EGFR WT IC_{50} 5110 nM

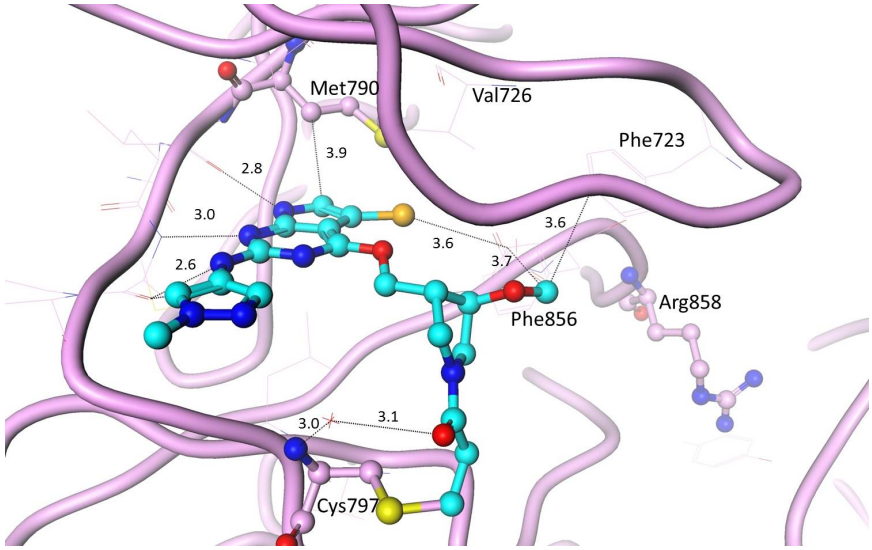

Figure 1: 1 a previously reported T790M mutant inhibitor that has exceptional selectivity over WT EGFR. The 1.9 Å co-crystal structure (PDB ID 5HG7) with EGFR T790M/L858R protein shows the ligand covalently modifying Cys797 of the EGFR protein as designed. The core also forms the classic donor-acceptor-donor motif to the kinase hinge region. Also highlighted is the gatekeeper residue, Met790. IC_{50} data is from cell-based assays.

Furthermore, by virtue of its weakly electrophilic acrylamide warhead, the broad proteome reactivity of **1** was significantly reduced relative to previous covalent EGFR inhibitors possessing more reactive warhead groups[8]. While **1** possessed characteristics desirable in a clinical candidate, its potency against the two original activating mutants of EGFR (L858R and the exon19_deletion (Del)) was mixed. Recognizing the physicochemical property limitations of the pyrrolopyrimidine series in improving Del potency without compromising the excellent

attributes of **1** (substitution of the halogen with an aromatic ring led to improved Del but with an increase in clearance due to high logD), an alternative chemical series was pursued. Herein, we describe our efforts applying the principles of affinity-driven potency and low intrinsic electrophile reactivity to i) increase Del potency while retaining potency against the T790M mutants and selectivity over the WT EGFR); ii) improve broad protein kinase selectivity across the kinome and iii) maintain excellent ADME properties suitable for once daily oral dosing in patients.

Results and Discussion:

To identify suitable chemical leads, a directed screening approach was applied. The lead generation screening strategy was to screen known *reversible* kinase inhibitors from the Pfizer compound collections, identify hits that were selective for T790M over the WT EGFR, and then append a warhead onto selected scaffolds (as informed by computational modeling using a T790M EGFR co-crystal structure[6d]). From screening a diverse kinase targeted library set of approximately 20,000 compounds, a purine containing lead was identified, compound **2** (Figure **2**)[9]. **2** exhibited EGFR T790M/L858R double mutant potency with an IC_{50} of 78 nM and WT selectivity of 76 fold in a biochemical kinase assay. However despite acceptable passive permeability ($1.9x10^{-6}$ cm/s), when tested in a cellular context (NSCLC derived H1975 line expressing T790M/L858R double mutant (DM)), **2** was inactive even at 10 μM, illustrating the opportunity for covalent inhibitor modality. As in our previous work[1], increasing potency by optimizing non-covalent binding affinity, using an estimated Ki assay (K_i^{est}) to assess progress,

and incorporating *weakly* reactive aliphatic warheads (as measured using a glutathione assay) were the focus of the optimization program[10].

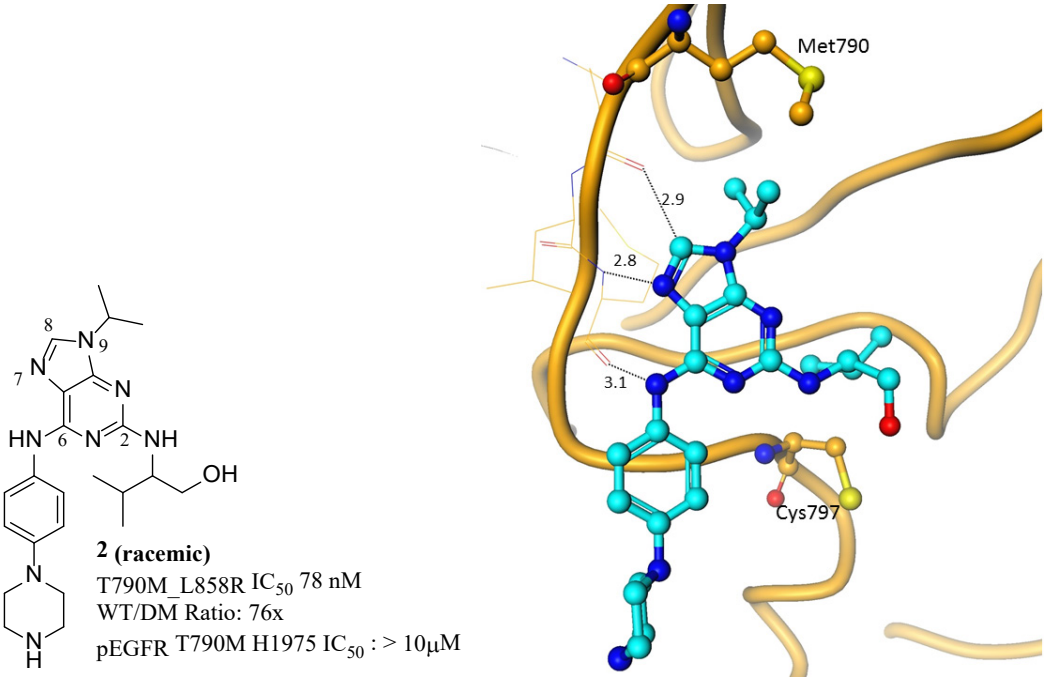

Figure 2. Modeled docking of screen hit **2** into the EGFR T790M/L858R protein (PDB ID 5HG7). Note core hinge interactions including polarized C(8) C-H bond. The close proximity of the C(2) vector to target Cys797 indicated the best vector on which to append an electrophile.

To determine how to best incorporate a suitable electrophile, binding of **2** was modeled using T790M/L858R EGFR crystal structure. The predicted binding mode (Figure **2**) involved a tridentate hydrogen bonding interaction to the kinase hinge region, consisting of two formal hydrogen bonds (with the core N(7) acting as an acceptor and the aniline NH as a donor), and a polarized C–H bond at the C(8)-position acting as a second hydrogen bond donor (interacting with the carbonyl of hinge residue GLN791). The N(9) isopropyl group was in close proximity to the gatekeeper methionine residue which was predicted to be driving selectivity over WT EGFR, and the C(2) valinol group appeared to be in closest proximity to the target Cys797 residue

offering a vector for warhead incorporation. SBDD suggested a pyrrolidine linker was suitable to place an acrylamide warhead in close proximity to the target cysteine. Key examples are shown in Table **1**.

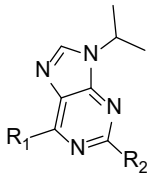

Compound ID	R1	R2	K_i^{est} (nM) [a]	k_{obs}/I ($M^{-1}s^{-1}$) [a]	H1975 IC_{50} (nM) [c]	A549 IC_{50} (nM) [c]	WT/ DM	LogD	Rel [d] GSH $T_{1/2}$
3	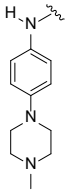	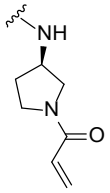	32	3953 (1 μM) [b]	29	387	13	2.5	ND
Ent-3	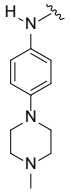	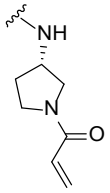	164	258 (5 μM) [b]	280	> 10,000	> 35	1.8	> 15
4	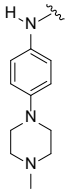	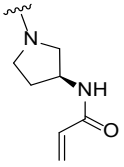	9	11,886 (0.1 μM) [b]	19	277	15	2.2	> 22
Ent-4	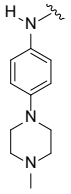	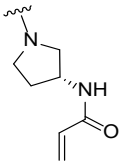	161	53 (5 μM) [b]	ND	ND	-	2.0	ND
5	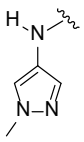	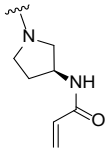	36	4452 (1 μM) [b]	52	652	13	2.3	> 18

Ent-5	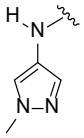	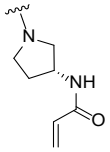	183	97 (5 μM) [b]	ND	ND	-	2.7	ND
6	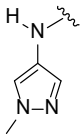	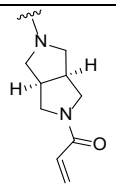	85	2041 (1 μM) [b]	49	805	16	2.2	> 15

Table 1: **Summary Early Purine Examples**. a) K_i^{est} and k_{obs}/I derived as previously published; b) Inhibitor concentration at which the k_{obs}/I is calculated c) H1975 and A549 IC_{50} represent activities against T790M/L858R and WT EGFR respectively; d) Rel GSH $T_{1/2}$ represents the intrinsic warhead reactivity expressed as the fold-change in half-life of parent compound in a glutathione stability assay relative to that of canertinib ($t_{1/2}$ *ca:* 21 min).

As shown in Table **1**, the pyrrolidine-based linkers contained within **3** and **4** showed promising early data with K_i^{est} values approaching our 10 nM goal. Preference for the 3-acrylamido pyrrolidine warhead was observed, based both on higher affinity (as determined by extrapolated K_i^{est}) and a significant increase in the rate of covalent modification (measured k_{obs}/I) observed with **4** compared to **3**. An enantio-preference was observed for both pyrrolidine based linkers, as illustrated when comparing enantiomers of compound **3** and **4**. These observations were in agreement with modeling predictions that placed the exocyclic (*S*)-acrylamide in closer proximity to the target Cys797 (see Figure **3**).

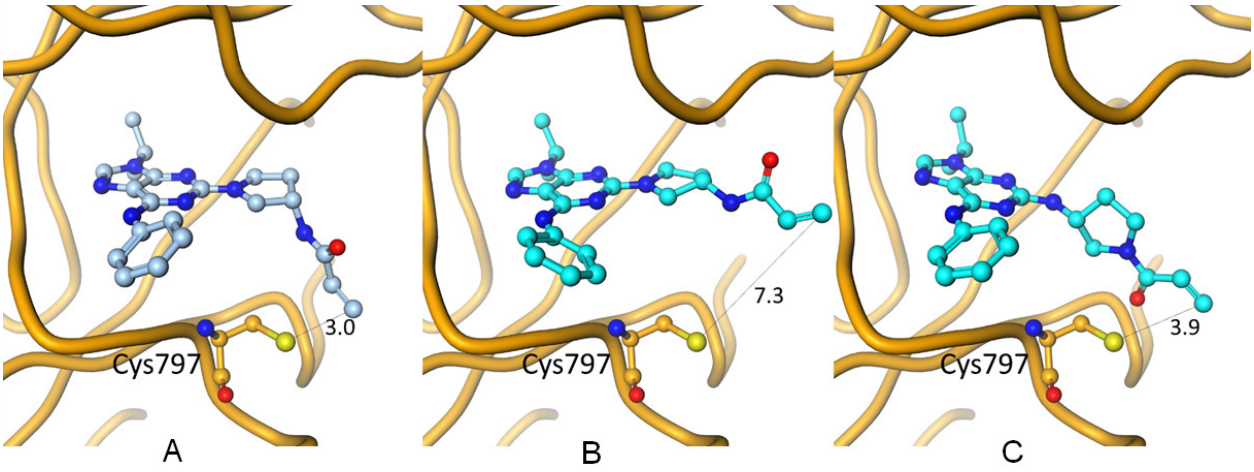

Figure 3. Modeled docking of simplified compounds containing pyrrolidine linked warheads into the EGFR T790M/L858R protein (PDB ID 5HG7). Distance of highlighted CYS797 to the acrylamide is shown. A and B) linker from **4** showing "*pseudo-axial*" and "*pseudo-equatorial*" warhead conformations respectively; C) isomeric pyrroldine linker from **3**.

Together with its very low intrinsic reactivity (relative GSH half-life of 22-fold), high potency in both biochemical and H1975 cell assays (9 nM and 19 nM, respectively), a high k_{obs}/I value approaching 12,000 $M^{-1}s^{-1}$ and 15 fold selectivity over WT EGFR, the 3-amino pyrrolidine derivative contained in **4** represented the best linker motif, and formed the basis for further design optimization.

Anilines are known potential toxicophores[11] and the high molecular weight, high logD and basic nature of the bis-aniline fragment contained in **4** (ACD calc *p*Ka 7.9) constrained the molecule's physiochemical profile and likely contributed to observed liabilities including ion-channel activity, poor permeability and poor LipE[12]. Thus, an early optimization goal was to replace the aniline fragment with a pyrazole moiety (as shown in Table **1**, compounds **5, 6**), leveraging knowledge derived from program to discover **1**[1]. Compound **5** with a 3-amino pyrrolidine linker afforded activity with a K_i^{est} of 36 nM and an IC_{50} of 52 nM in the H1975 cell assay, while

retaining WT selectivity and low reactivity. However, with a relatively low k_{obs}/I of 4452 $M^{-1}s^{-1}$, more potency could be obtained by improving alignment of the warhead to the cysteine[13]. The bicyclic pyrrolidine linker of **6** also afforded activity but offered no benefit over the simpler linker of compound **5.**

Modeling of lead compound **5** suggested that the acrylamide would prefer to adopt a less favored, "pseudo-*axial*" conformation in order to place the warhead proximal to Cys797 for facile covalent modification (Figure **3a**). As a result of the incurred strain energy penalty (calculated at 1.3 kcal/mol in solution phase), it was hypothesized that a potency gain would be realized if the molecule could be modified to favor this conformation. Replacement of a pyrrolidine hydrogen with a fluorine is known to impart a gauche effect, whereby an adjacent electronegative substituent prefers to be in a gauche orientation[14]. Addition of fluorine onto the 4-position of the pyrrolidine ring of compound **5** was calculated to result in a slight preference (by 0.1 kcal/mol) for the 3,4-*anti* conformation. In fact, fluorine introduction to give **7** resulted in a significant potency gain from both an affinity *and* inactivation rate perspective (Table **2**), with the k_{obs}/I increased to 62,982 $M^{-1}s^{-1}$. This reflected the less costly accessibility of the *anti* conformation and the improved orientation and proximity of the warhead relative to the cysteine for **7** compared to **5**.

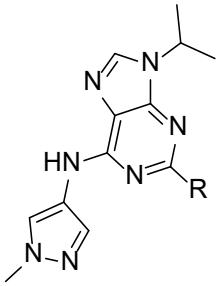

Compound	R	K_i^{est}	k_{obs}/I	H1975	A549	WT/DM	LogD	LipE [d]	Rel [e]

ID		(nM)[a]	($M^{-1}s^{-1}$) [a]	IC_{50} (nM) [c]	IC_{50} (nM) [c]				GSH $T_{1/2}$
5	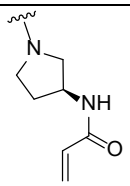	36	4,452 (1 μM) [b]	52	652	13	2.3	5.1	> 18
7	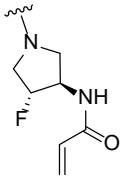	2	62,982 (0.05 μM) [b]	7	178	26	2.6	6.1	> 18
8	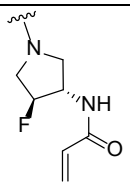	152	244 (5 μM) [b]	713	>10 uM	-	2.5	4.3	> 18

Table 2: **Effect of Fluorine Addition to Linker**; a) K_i^{est} and k_{obs}/I derived as previously published. b) Inhibitor concentration at which the k_{obs}/I is calculated. c) H1975 and A549 IC_{50} represent activities against T790M/L858R and WT EGFR respectively; d) LipE calculated from K_i^{est} and experimental logD; e) Rel GSH $T_{1/2}$ represents the intrinsic warhead reactivity expressed as the fold-change in half-life of parent compound in a glutathione stability assay relative to that of canertinib ($t_{1/2}$ *ca:* 21 mins).

A 1.5 Å cocrystal of compound **7** with EGFR L858R/T790M (with additional surface mutation V948R, distal from the ligand binding site, Figure **4**[15]) was obtained which confirmed the predicted *anti* conformation of the fluorine and the acrylamide. A small molecule X-ray structure also later confirmed the low energy state (see supporting information for small molecule crystal structure of **21,** Figures **SF1-SF3**). In addition, as predicted from docking experiments, the fluoro substituent of **7** is within 3.6 Å of the G-loop Phe723 and able to interact *via* a dipole-dipole interaction[16]; the cumulative result is a profound 10-fold increase in potency, *and* a lipE[17] increase of 0.8 relative to the *des*-fluoro analog. A high enantiomeric preference was observed as

the distomer (compound **8**) was more than 60 fold less potent against the T790M/L858R double mutant.

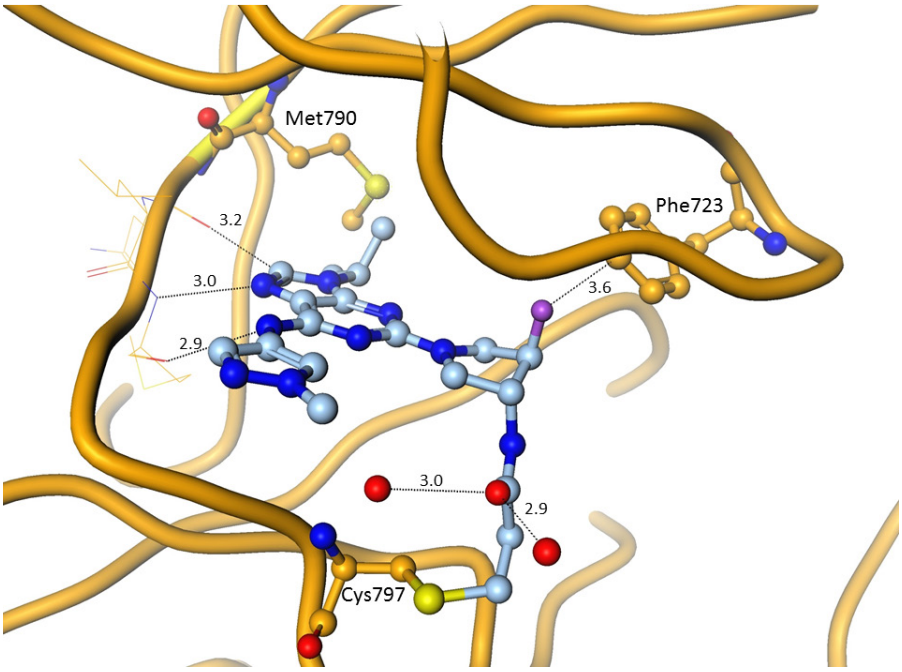

Figure 4. 1.5 Å Cocrystal Structure (PDB ID 5UG8) of compound 7 with EGFR_L858R/T790M Mutant (only the ligand binding site is shown). Note *anti* conformation of fluorine and warhead linker and apparent fluorine interaction with Phe723.

In the previously disclosed pyrrolopyrimidine work[1], addition of fluorines into warhead linkers was accompanied by an increase in intrinsic reactivity *via* lowering of the acrylamide LUMO through the inductive effect of the fluorine, as illustrated in Table **3** when comparing the compound pairs **9 - 10**, and **11 - 12**.

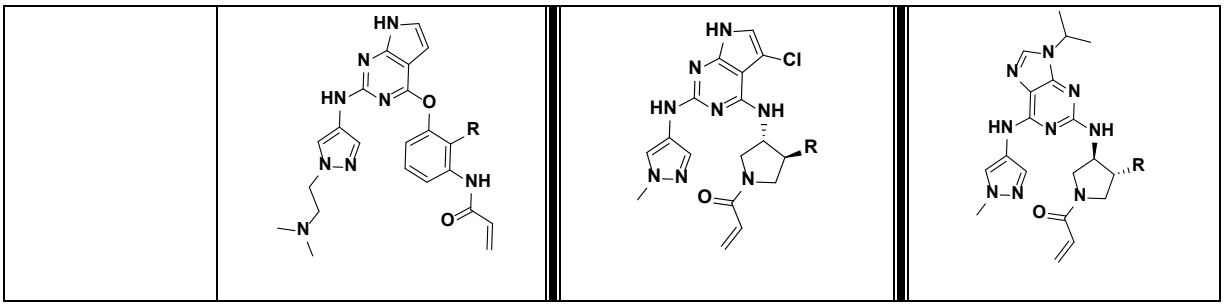

	R=H (9)	R=F (10)	R=H (11)	R=F (12)	R=H (13)	R=F (14)
T790M/L858R K_i^{est} (nM)	3	2	4	3	105	56
Rel GSH $T_{1/2}$ (fold change)	4	1	22	5	14	9

Table 3: Fluorine Introduction into the Warhead Linker. Fluorine introduction in pyrrolopyrimidine and early purine examples showed an increase in the relative intrinsic reactivity of the warhead. Rel GSH $T_{1/2}$ represents the intrinsic warhead reactivity expressed as the fold-change in half-life of parent compound in a glutathione stability assay relative to that of canertinib ($t_{1/2}$ *ca:* 21 mins).

Because a minimally reactive warhead was sought, this observed increase in intrinsic reactivity precluded advancement of these compounds. Similar results were seen in the purine series with the same fluorinated pyrrolidine linkers **13** and **14** (Table **3**) where fluorine introduction led to an increase in reactivity, with the GSH relative half-life dropping from 14 to 9 fold. *However*, unlike these examples, it was predicted that the *anti* conformation of the 3-acrylamido-4-fluoropyrrolidine of **7** would *not* significantly increase the reactivity of the warhead (Table **2**) when the potential for orbital overlap between the C-F bond and the nitrogen of the acrylamide was considered. In examples where an increase in reactivity was observed, it was possible to align the σ* of the C-F bond with the nitrogen lone pair of the acrylamide, which would lower the LUMO energy and increase the reactivity of the warhead (Figure **5a**).

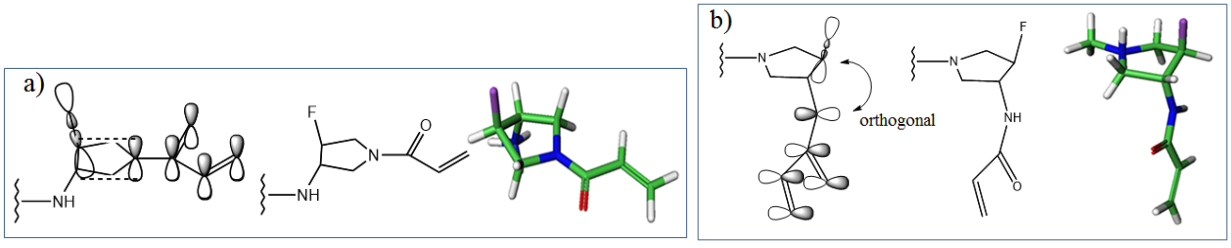

Figure 5: a) Activating Fluorine: Overlap between warhead nitrogen NB-orbital and σ* orbital of C-F bond of **14** increases the reactivity of the Michael acceptor. **b) Neutral Fluorine:** Orthogonal orbitals have minimal interaction which resulted in little effect on intrinsic reactivity of **7**.

In the case of compound **7**, the orthogonal orientation between the warhead nitrogen non-bonding (NB) orbital and the C-F σ* orbital reduces interaction with the electrons of the LUMO; as a result the fluorine would not be predicted to adversely impact the intrinsic reactivity (Figure **5b**). Upon testing in the glutathione based reactivity assay, fluorine introduction was found *not* to exhibit a measurable difference in intrinsic reactivity when comparing the relative GSH reactivity half-lives between **5** and **7** (Table **2**). Thus, fluorine addition was found to have a profound benefit by i) *anti* conformational preference, ii) a dramatic increase in potency, iii) increased interaction with the protein, and iv) no negative impact on the intrinsic reactivity. Compound **7** had moderate clearance with an exceptional EGFR mutant profile, possessing single digit nanomolar potency against all 4 mutants and 20 fold selectivity over WT EGFR. Thus, having optimized the warhead linker group, the series was evaluated for selectivity against the kinome.

Kinase Selectivity: The kinome selectivity for the simple pyrrolidine-linker compound **5** was moderate, with a hit-rate of 25% when assessed against a diverse 38 membered kinome panel (where a hit is defined as > 50% inhibition in biochemical screening assay at 1 μM at K_m concentrations of ATP, see supporting information Table **ST2**). This is approximately the same for **1**. While addition of fluorine was beneficial from a potency and efficiency perspective, this change had a deleterious effect on the kinome selectivity with the hit-rate increasing to 43%. One possible explanation for the increase in off-target kinase activity is the observed interaction between the fluorine and Phe723. This Phe is well conserved throughout the kinome (67% of

kinases possess a Phe at this location) and specific interaction with it could result in an increase in kinase promiscuity. To improve upon this profile, a selectivity pocket afforded by hinge residue Leu792 (Figure **6**) was targeted. In many kinases (59% of the kinome), this hinge residue (H5) is either a larger Phe or Tyr, offering a strategy for selectivity by building a steric clash with those larger residues. Filling this pocket has been shown to achieve kinase selectivity for other kinase programs such as ALK[18], MPS-1[19] and LRRK2 which both possess a leucine residue at the corresponding hinge position.

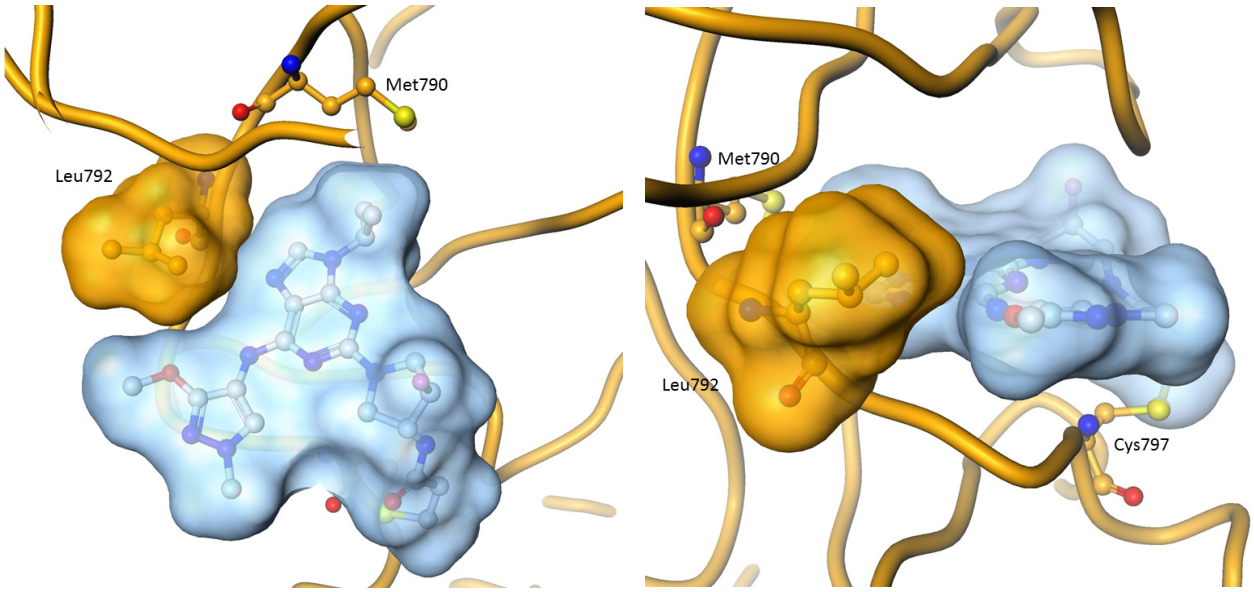

Figure 6: Co-Crystal Structure of 16 (1.3 Å, PDB ID 5UG9). The kinase selectivity pocket that is afforded *via* hinge residue Leu792 is illustrated. Many kinases (59%) have a large Phe or Tyr residue in this position, precluding pyrazole substitution. Filling this pocket with a methoxy group afforded an improved kinase off-target profile without significant detrimental impact on *in vitro* human microsomal intrinsic clearance.

Placing small groups (methyl, methoxy, ethyl) in this region afforded compounds **15-17 (**Table **4**). Addition of methyl (**15**), methoxy (**16**) or ethyl (**17**) all improved kinase selectivity, with compound **16** providing the best combined potency and lipE, with minimal impact on the *in vitro* microsomal intrinsic clearance or potency. Compound **16** showed activity against only two

kinases outside the Tec family both of which possess a leucine residue at the H5 hinge region, thus circumventing the selectivity strategy (see supporting information Table **ST2**).

Compound ID	Structure	K_i^{est} (nM)[a]	k_{obs}/I ($M^{-1}S^{-1}$)[a]	H1975 IC_{50} (nM)[c]	A549 IC_{50} (nM)[c]	WT/ DM	LogD	LipE[d]	hLM Cl_{int} (µl/min/mg)[e]	Kinome hitrate (%)[f]
7	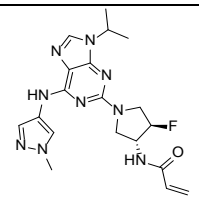	2	62,982 (0.05 µM)[b]	7	178	26	2.6	6.1	25	58
15	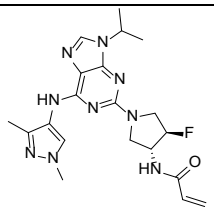	17	5699 (1 µM)[b]	26	1,450	56	2.6	5.2	30	13
16	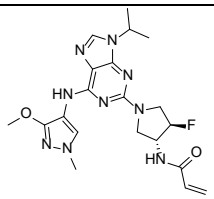	8	28,437 (0.1 µM)[b]	5	160	32	2.6	5.5	32	13
17	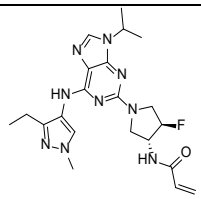	19	6415 (1 µM)[b]	7	649	89	3.5	4.2	81	8

Table 4: ***in vitro* Profiles for Pyrazoles Designed to Improve Kinase Selectivity**. a) K_i^{est} and k_{obs}/I derived as previously published. b) Inhibitor concentration at which the k_{obs}/I is calculated. c) H1975 and A549 IC_{50} represent activities against T790M/L858R and WT EGFR respectively. d) LipE calculated from K_i^{est} and experimental logD. e) hLM: Human Liver Microsomal intrinsic clearance. f) Kinase hitrate expressed as % kinases that showed >50% inhibition at 1 µM inhibitor at K_m levels ATP from a diverse 38 membered panel.

Single Mutant Potency: One of the primary objectives for this work was to improve the potency against the Del mutation. Current clinical T790M inhibitors are least potent against this mutant form compared to other single (L858R) and double T790M mutants, and this was also seen in our previous work using the 5-chloro-pyrrolopyrimidine scaffold, where **1** was 11 fold less potent against Del than T790M/L858R (PC9 and H1975 cell lines, respectively)[1]. Plotting double mutant (T790M/L858R, H1975) *vs* single mutant (Del, PC9) cell potency highlights the differentiation between the pyrrolopyrimidine and the purine scaffolds (Figure **7**). In general, the purine series (shown in blue) provided equivalent potency or better for Del mutation, in contrast to the pyrrolopyrimidine series (shown in orange) where a 10-fold loss was generally observed.

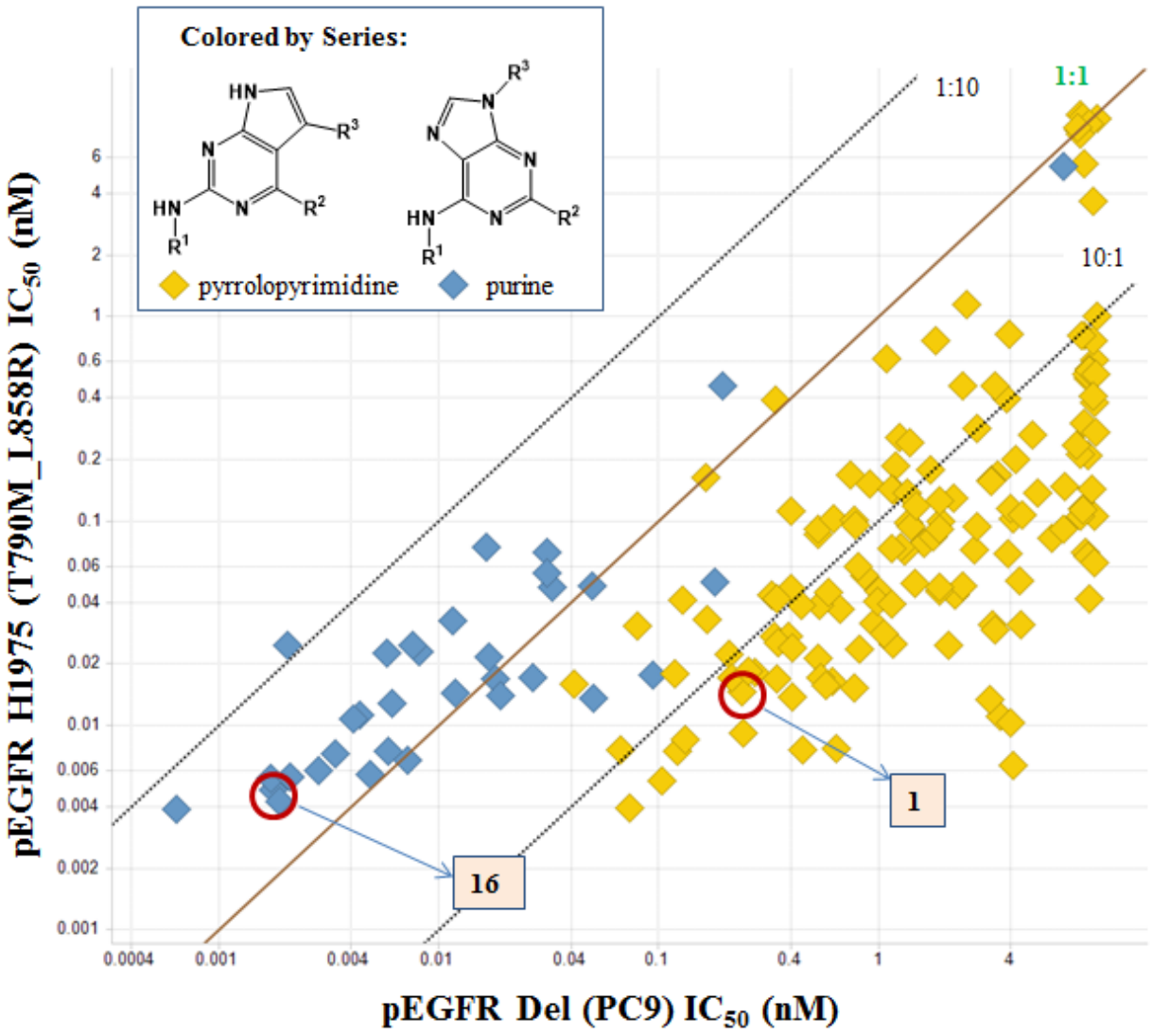

Figure 7: Single Mutant *vs.* Double Mutant Potency. Plot showing series potencies against the T790M/L858R double mutant (H1975) and the Del (PC9) single mutant highlighting the superior Del mutant coverage of the purine series (blue) over the previous work's pyrrolopyrimidine series (orange).

When assessed against the single mutations (L858R and Del) and double mutations (T790M/L858R and T790M/Del), the purine series exhibited higher potency against *all* key mutant isoforms with more than 15-fold better potency against Del than our previously disclosed compound **1**. Single digit nM potencies were observed across each of the four mutant EGFR NSCLC cell lines for **16** (Table **5**).

Compound	H1975 (T790M/L858R)	PC9-DRH (T790M/Del)	PC9 (Del)	H3255 (L858R)	A549 (WT)	WT ratio*
1	13	7	140	21	5110	36
7	7	2	9	2	178	20
15	26	4	16	9	1450	56
16	5	1	2	2	160	32
17	7	3	*ND*	*ND*	649	89

Table 5: **pEGFR Potency Data (IC_{50}, nM).** The purine series example **16** displayed a flatter potency profile across the EGFR mutants relative to compound **1** from previous work where the Del mutation was hardest to cover. (*ratio expressed using lowest EGFR mutant potency. *ND* not determined)

N(9) Substituent and EGFR Wild-Type Selectivity: With broad kinase selectivity and the desired EGFR mutant profile in hand, efforts were then focused on investigating the purine N(9) substituent and its impact on WT EGFR selectivity. The N(9) group was considered a driver for WT selectivity because of its close proximity to the gatekeeper residue. Analysis of N(9) ^{i}Pr purine co-crystal structures showed that in order to bind in the active site of WT EGFR, rotation of the isopropyl group was necessary to avoid an electrostatic clash between the lipophilic ^{i}Pr group and the polar threonine gatekeeper. This was confirmed with a co-crystal of reversible acetate analog **18** bound in WT EGFR (Figure **8**).

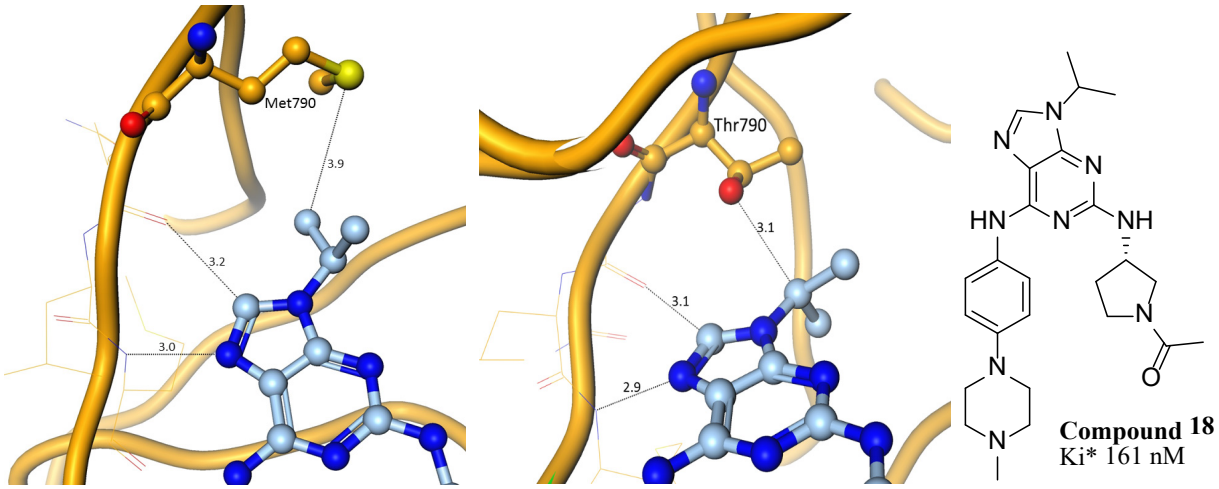

Figure 8: N(9) ^{i}Pr Rotation on Binding to WT EGFR. Co-crystal structures of compound **18** in EGFR L858R/T790M (left, 1.3 Å resolution, 5UGA) and WT EGFR (right, 2.1 Å resolution, 5UGB) illustrated the orientation of the ^{i}Pr group relative to the gatekeeper residue: note the rotation of the N(9) ^{i}Pr when bound in the WT pocket. *Measured K_i in T790M/L858R double mutant.

Whereas in the L858R/T790M structure, the two isopropyl methyl groups of the ligand orient themselves toward the gatekeeper residue with productive VDW interactions, Thr790 in the WT structure precludes this both sterically and electrostatically. The *tert*-butyl (^{t}Bu) substituted analog was predicted to have increased WT selectivity, as modeling predicted that the larger substitution removes the possibility of the N(9) group to offer a hydrogen toward Thr790. Due to the critical nature of this N(9)-gatekeeper interaction, ethyl and methyl analogs were also synthesized for comparison (see PDB ID 5UGC). Data for key examples are shown in Table **6**, together with selected ADME properties.

Compound ID	Structure	K_i^{est} (nM)	H1975 IC_{50} (nM)	A549 IC_{50} (nM)	WT/ DM	LogD	LipE (H1975)	LipE (WT)	RRCK (10^{-6} cm/sec)	HLM Cl_{int} (µl/min/mg)	hHep (µl/min/MM)

16	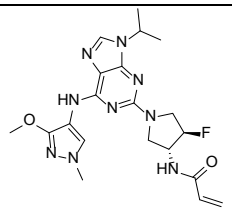	8	5	160	32	2.6	5.7	4.2	18	31	23
19	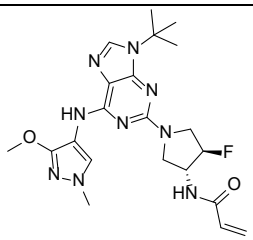	18	17	673	40	3.3	4.5	2.9	16	65	ND
20	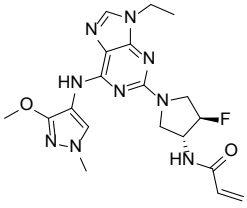	6	8	83	11	2.3	5.8	4.9	12	9	5.6
21	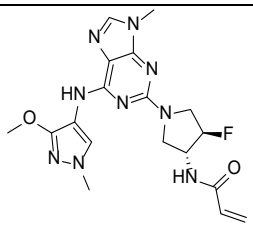	13	12	307	26	2.0	5.9	4.5	9	8	3
22	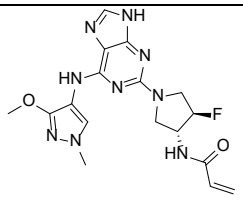	ND	675	750	1	1.8	4.4	4.3	2	8	ND

Table 6: Purine N(9) variation. The larger *tert*-butyl group afforded the highest selectivity margin over WT but at the expense of higher clearance and lower LipE. K_i^{est} derived as previously published. H1975 and A549 IC_{50} represent activities against T790M/L858R and WT EGFR respectively. LipE calculated from IC_{50} and experimental logD. HLM: human liver microsomal clearance. RRCK: permeability as measured using low-efflux MDCK-LE cell line. hHep: human hepatocyte intrinsic clearance.

Introduction of the ^{t}Bu N(9) group (**19**) afforded an incremental increase in the WT/DM ratio, but concomitant increase in clearance driven by the extra lipophilicity prevented progression. Generally across a number of purines, ^{t}Bu N(9) *did* result in the best WT selectivity when compared with other alkyl groups (^{t}Bu > iPr ≈ Me > Et as seen in the pairwise plot, Figure **9**), with ^{i}Pr and Me N(9) being approximately equal, and Et being the least selective over WT.

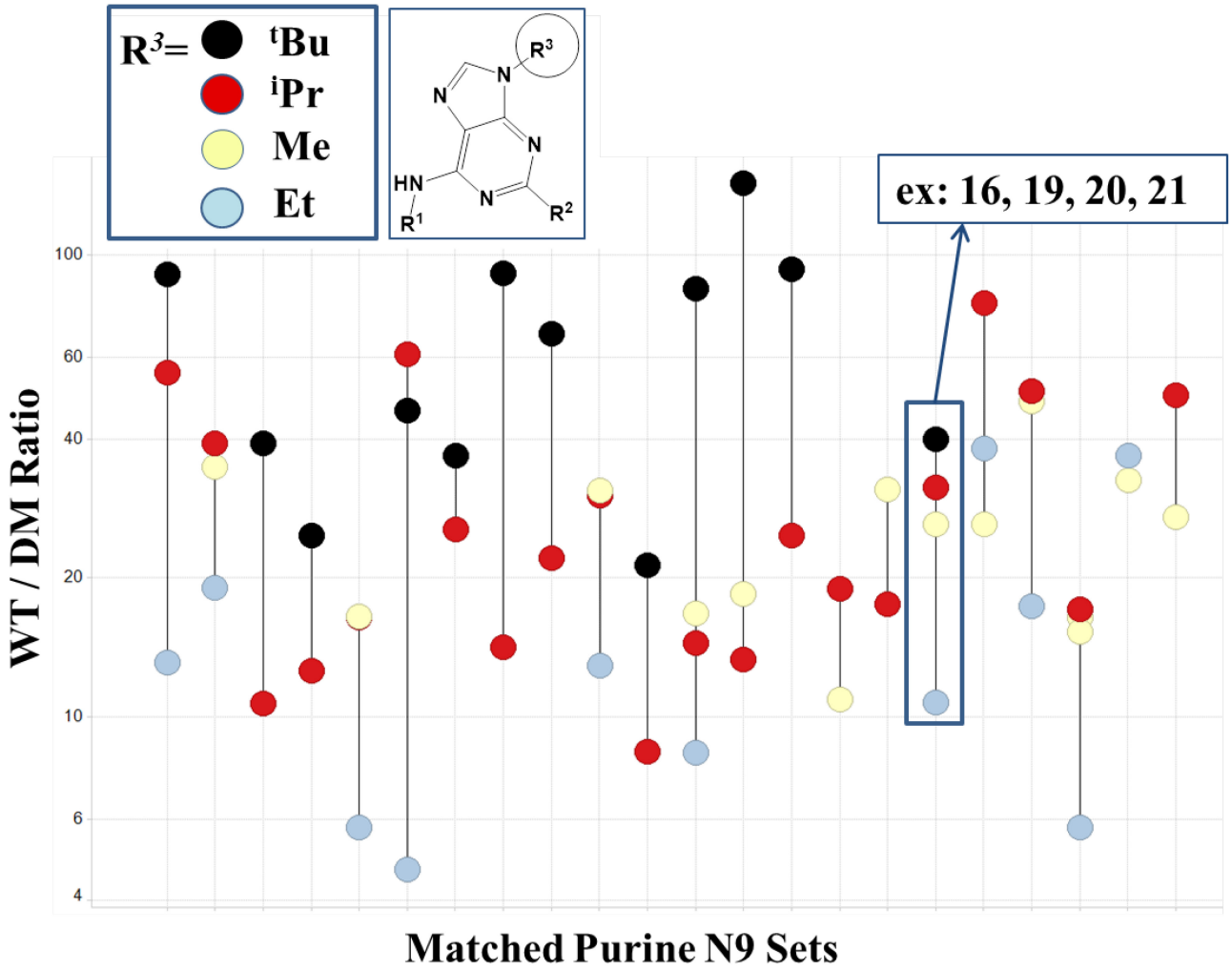

Figure 9: Matched Pairwise Plot by N(9) Substituent. Plot illustrated cellular pEGFR WT selectivity seen by varying N(9) substituent size; the larger *tert*-butyl group consistently afforded the highest selectivity. The methyl substituent examples go against the trend and in many cases *improved* WT selectivity relative to the corresponding ethyl or isopropyl analog.

When considered from a LipE perspective, the ^{t}Bu N(9) analog **19** had a much lower LipE of 2.9 compared to the methyl analog **21** (LipE 4.5) *vs.* WT EGFR for reasons discussed above. The ethyl analog **20** was able to bind with the ethyl group orthogonal to the core and is buried in a hydrophobic region of the G-loop, making no steric clash with the WT or T790M proteins, hence WT selectivity is reduced (supporting information, Figure **SF4**). The biochemical and cellular potency of methyl N(9) compound **21** was within two-fold of the isopropyl analog **16**. However, **21** (most likely because of the reduction in logD) possessed greatly improved *in vitro* clearance (hLM 8 µL/min/mg and hHEP 3 µL/min/MM), high permeability (RRCK[21] 9 x10^{-6} cm/sec) and increased LipE. Additionally, this was accompanied by a loss of CYP450 time-dependent inactivation (TDI) that was observed for examples with higher logD (data not shown). With the improved physiochemical profile (MW 415 g/mol, tPSA 115, *p*Ka 3.53, logD 2.0) and resultant superior ADME properties, excellent potency and 26-fold selectivity over the WT, the N(9) methyl analog **21** (**PF-06747775**)[22] was deemed to have the best overall balance of properties and was selected for full characterization.

Pre-Clinical Evaluation Overview of 21.

The covalent inhibitory potency (k_{inact}/K_i 350,000 – 610,000 $M^{-1}s^{-1}$) of **21** was high for both double mutant proteins, significant for single activating mutant proteins (k_{inact}/K_i 68,000 – 103,000 $M^{-1}s^{-1}$), and weak for WT EGFR (k_{inact}/K_i = 12,000 $M^{-1}s^{-1}$) (full characterization details included in supporting information, Table **ST5**). Cellular potency assessment of **21** against the EGFR single mutants (Del and L858R) and the double mutants (T790M/Del and T790M/L858R) revealed single digit nanomolar IC_{50}s for all but the T790M/L858R isoform which was had an IC50 of 12 nM (Table **7**). Selectivity for inhibition of the four activating EGFR mutants *vs.* WT was 26 fold when compared to the least active EGFR mutant (T790M/L858R H1975). Compared

to our previously disclosed compound **1**[1], the mutant EGFR isoform inhibition potency was improved for both single mutants. Other clinical T790M inhibitors Tagrisso (**AZD9291**[6f], **23**), and rociletinib (**CO1686**[6g], **24**) (from Astra Zeneca and Clovis, respectively) are included for comparative reference. When the WT selectivity was assessed against the weakest activating mutant activity, **21** was nearly ten-fold better than **23** (26- *vs* 3-fold selective) and slightly better than **24** (26- *vs* 20-fold selective). Also shown is first generation quinazoline inhibitor erlotinib[23] (**25**), which despite being potent against the single EGFR mutants lacks potency against the T790M double mutants. Inclusion of a warhead onto a typical quinazoline scaffold (**26**) rescues the T790M activity, but with no selectivity observed over WT.

Compound ID	Structure	L858R/T790M IC_{50} (nM)	Del/T790M IC_{50} (nM)	L858R IC_{50} (nM)	Del IC_{50} (nM)	WT IC_{50} (nM)	Ratio (WT / least potent target)*
		H1975	*PC9-DRH*	*H3255*	*PC9*	*A549*	
21	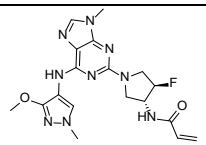	12	3	4	5	307	26
1	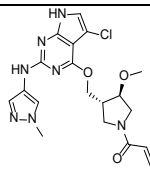	13	7	21	140	5,100	36
23 (AZD9291) *(AstraZeneca)*	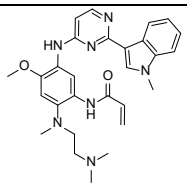	15	13	36	56	152	3
24 (CO1686) *(Clovis)*	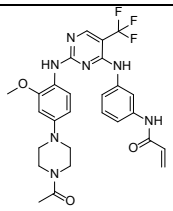	16	9	46	79	1598	20

25 (Erlotinib)	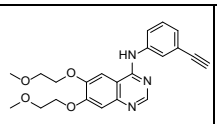	9003	9736	10	11	11	1
26	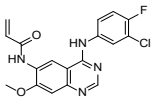	7	ND	1	1	6	1

Table 7: *in vitro* profile comparison of pEGFR IC_{50} (nM) in NSCLC cell lines for 21 and clinical EGFR_T790M inhibitors. *Cell ratio expressed as WT / least potent target, except for Erlotinib which is considered on single mutant data.

Kinase selectivity of **21** was screened using enzyme assays against a total of 273 kinases constituting approximately 50% of the human catalytic protein kinome (supporting information, Table **ST3**). Under assay conditions of ATP concentration equal to K_m with 1 μM of **21**, 15 kinases of the 273 tested were inhibited > 50% (supporting information, Table **ST4**). These 15 kinases were tested in follow up enzyme assays where conditions were modified by increasing the ATP concentration to simulate cellular ATP levels. Under these more physiologically-relevant conditions, 7 kinases showed > 50% inhibition (ERBB4, BTK, BMX, TXK, TEC, ROS, and ACK/TNK2). It is notable that of these 7 kinases, the first 5 listed have a cysteine residue in the same position as that of EGFR-Cys797, the residue that is targeted for covalent modification by **21**, and hence these kinases are subject to time-dependent irreversible inhibition. Only two of the 6 tested *non*-cysteine kinases (FER and ACK/TNK2) were inhibited with moderate potency, albeit with a selectivity margin of > 9-fold as compared to EGFR mutant target cellular potencies of **21**.

To extend this selectivity analysis to the more physiologically-relevant setting of intact cells, selected kinases were tested for inhibition by **21** in the cellular context (supporting information, Table **ST4)**. Four tested kinases (BTK, JAK3, ROS, and BLK) showed weak inhibition in the

cellular context. Collectively, the kinase selectivity analysis of **21** using standard enzymatic and cellular formats identified 7 kinases of the 273 tested (ERBB4, ERBB2, BMX, TXK, TEC, FER, and ACK/TNK2) with the potential for inhibition by **21,** yielding a high selectivity index of 97%.

Proteome Reactivity Assessment: In order to assess the total cellular proteome reactivity of **21,** (and to compare relative to **1**), an alkynylated variant was synthesized (at a position that produced a minimal change in terms of target protein reactivity and specificity, designated here **P_21**, figure **10**)[24]. The physiochemical properties of this chemical probe including its cellular IC_{50} against WT and double mutant EGFR, k_{obs}/I and GSH reactivity closely matched that of the corresponding parent molecules making this probe an adequate surrogate of its parent inhibitor (supporting information, Table **ST6)**. The generation and characterization of the chemical probe for **1**, called here **P_1**, has been previously described[1]. The reactivity of these two probes was compared to that of a chemical probe based on **26** (**P_AQ –** see Table **7**), a quinazoline-based covalent second generation pan-ERBB2 inhibitor, which contains a similar Michael acceptor acrylamide. Initial experiments were performed in the biologically relevant H1975 lung cancer cells, as this line expresses the double mutant L858R T790M form of EGFR. The *in situ* reactivity of these three probes was assessed in a competitive mode by gel-based analysis (Figure **10**). We were gratified by the lack of proteome-wide reactivity observed with the chemical probe **P_21** and **P_1** compared to **P_AQ** in both the particulate and soluble proteomes. In fact, for **P_21** the only protein that reacts and competes with parent inhibitor **21**, would be predicted to be EGFR (marked with *). Finally, **P_21** displays even less proteome reactivity that **P_1**

under these conditions highlighting the exquisite selectivity and reactivity of this third-generation T790M inhibitor.

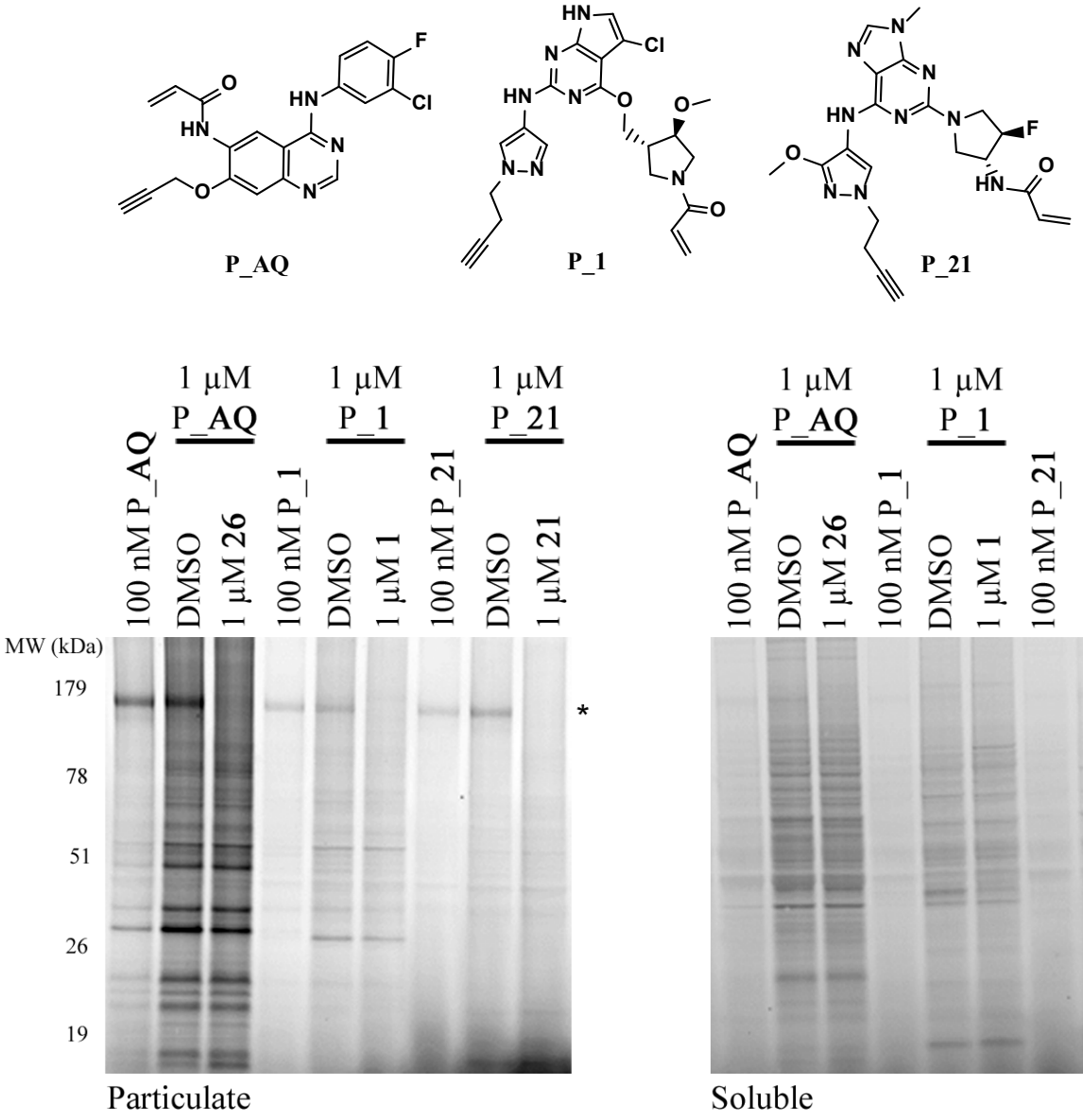

Figure 10: Competitive *in situ* labeling profiles of 1 µM of each chemical probe P_1 and P_21, *vs.* a representative aminoquinazoline probe, P_AQ. H1975 cells were treated 1 µM parent inhibitor (**26, 1**, **21**) or an equal amount of DMSO for 2 hours. Next, 1 µM of the corresponding chemical probe is added for 3 hours. Representative proteome labeling profiles are also generated with 100 nM of each chemical probe for 3 hours. After labeling, cells are harvested, lysed and separated into particulate (left) and soluble (right) proteomes. Equal amounts

of protein lysate were reacted with azide-rhodamine and covalently labeled proteins were revealed by gel-based fluorescence (gels are shown in grayscale). * Highlights a protein in the particulate proteome predicted to be EGFR by molecular weight that is fully competed with parent inhibitor.

Microsomal and hepatic *in vitro* clearance was species dependent, with mouse and rat showing high clearance and dog and human showing low clearance (Table **8**), with little or no inhibition of cytochrome P450 isoforms. Blood stability was high across all species, and **21** was found to distribute preferentially into plasma relative to whole blood in all species except dog (blood to plasma ratio ranged from 0.5-1.2). Plasma protein binding was relatively low. Metabolite identification using hepatocytes and microsomes revealed no active metabolites were observed. Glutathione adducts and demethylation were the major observed pathways (supporting information, Figure **SF5** and Table **ST8**).

	Mouse	**Rat**	**Dog**	**Human**
Microsomal $Cl_{int,app}$ (mL/min/kg)	74	141	3	< 6
Hepatic $Cl_{int,app}$ (mL/min/kg)	196	183	17	3
Blood Half Life (mins)	306	237	279	348
Protein Binding (f_u)	0.20-0.49*	0.22	0.75	0.27
Human Cytochrome P450 inhibition (3A4, 2D6, 2C8, 2C9, 1A2)	< 30% @ 10 μM			
CL_p (mL/min/kg)	53	49	12	-
V_{dss} (L/kg)	1.48	0.66	0.94	-
$T_{1/2}$ (hours)	0.56	0.28	1.3	-
F %	60	11	66	-

Table 8: Additional key *in vitro* and single–dose PK summary for **21**. *Fu in mice was found to be strain dependent. Intravenous clearance, V_{dss} and $T_{1/2}$ data assessed for mouse (female Nu/Nu), rat (male Wistar-Han) and dog (male beagle) using a 1 mg/kg solution. Bioavailability (F %) determined *via* dosing a 1 mg/kg crystalline suspension in mouse, 30 mg/kg in rat and 3 mg/kg in dog. Half-life based on the terminal β-phase.

Following *i.v.* administration at 1 mg/kg to mice, rats and dogs, **21** exhibited a moderate to high plasma clearance, and low steady state volume of distribution (Vd_{ss}), resulting in a short plasma half-life (CL_p, Table **8**). After oral dosing in preclinical species, **21** was rapidly absorbed with low to moderate oral bioavailability, which is believed to be driven by first pass metabolism (based on rat portal vein studies). In preclinical species, hepatic clearance was predominant when compared to non-hepatic clearance. The route of clearance was discerned by scaling the hepatic blood clearance utilizing the CL_{int} obtained from non-clinical species hepatocytes, the blood-to-plasma ratio, and the free fraction in plasma as opposed to the clearance observed in intravenous studies. In all non-clinical species tested, the clearance scaling method from hepatocytes predicted approximately 2 fold or less than what had been observed *in vivo* for **21**. Hence *in vitro* human hepatocyte scaling was deemed sufficient for the human clearance prediction. In humans, the major route of clearance of **21** is likely to be the hepatic metabolic clearance, which includes oxidative metabolism and glutathione conjugation *via* glutathione S-transferase[25]. The human clearance was predicted to be approximately $1/20^{th}$ to $1/30^{th}$ of hepatic blood flow and the predicted terminal half-life range was 12 to 13 hours. Oral bioavailability was predicted to be moderate (~80%) with a Tmax of ~4 hours. Details of the full evaluation of **21** *in vivo* using pharmacokinetic/pharmacodynamic (PK/PD) and tumor growth inhibition (TGI) studies will be disclosed in a separate publication.

Nonclinical safety profiling of **21** was also conducted. An off-target assessment was performed *in vitro* at 10 μM against a broad panel of receptors, enzymes, and ion channels (Cerep, Poitiers, France) where **21** exhibited less than 50% effect or inhibition against all non-kinase targets (supporting information, Table **ST7**). Assessment of the effects of **21** on the hERG[26] current showed IC_{50} > 100 μM, and the Ames mutagenicity evaluation was negative. Cardiovascular (i.e., blood pressure, heart rate and electrocardiogram measurements), pulmonary and central nervous systems functions were all assessed *in vivo* in a battery of single and repeat-dose safety pharmacology studies in rats and dogs with no effects (data not shown). Collectively, these results suggest minimal potential for secondary (off target) pharmacology. The *in vivo* toxicity profile of **21** was characterized in repeat-dose studies in rats and dogs (91 days duration). Compound **21** was well tolerated with no body weight loss. Compound-related effects at higher exposures were of an epithelial origin in the expected target organs (e.g., skin and gastrointestinal tract) at concentrations shown to inhibit WT EGFR, which reversed with cessation of dosing.

Synthetic Chemistry: In support of lead optimization, our initial goal was to achieve a modular and flexible route that allowed us to vary substitution at N(9), C(6) and C(2) of the purine scaffold. The synthesis of compound **4** (Scheme **1**) is representative of our initial efforts in this series. Both Mitsunobu and alkylation methods favored N(9) substitution but provided significant amounts of N(7) alkylated material that required chromatographic separation. In the case of anilinopiperazine **29**, S_NAr displacement at the C(6) position could be achieved with high selectivity under acidic conditions, but for other fragments (e.g., amino pyrazoles) S_NAr under basic conditions (DIPEA, DMSO) proved optimal. Compound **30** was typical of 6-amino

substituted purines in this series in that it was not sufficiently electrophilic to undergo S_NAr displacement at C(2) in good yield. As a result, Buchwald-Hartwig type aminations were investigated, and after significant reaction optimization it was found that the palladium precatalyst SK-CC02-A provided excellent reactivity across a range of amine nucleophiles. The doubly amine substituted intermediates, such as compound **32**, were then readily deprotected. Acylation to form acrylamide **4** using acryloyl chloride under Schotten-Baumann conditions provided only moderate yields. Similar yields were typically observed using activating reagents and acrylic acid. Our observations of these reactions suggest that at least two factors contribute to the difficult acryloylation, a) poor solubility of the intermediate free-based amine and b) covalent reaction of the free-based amine with the desired acrylamide product.

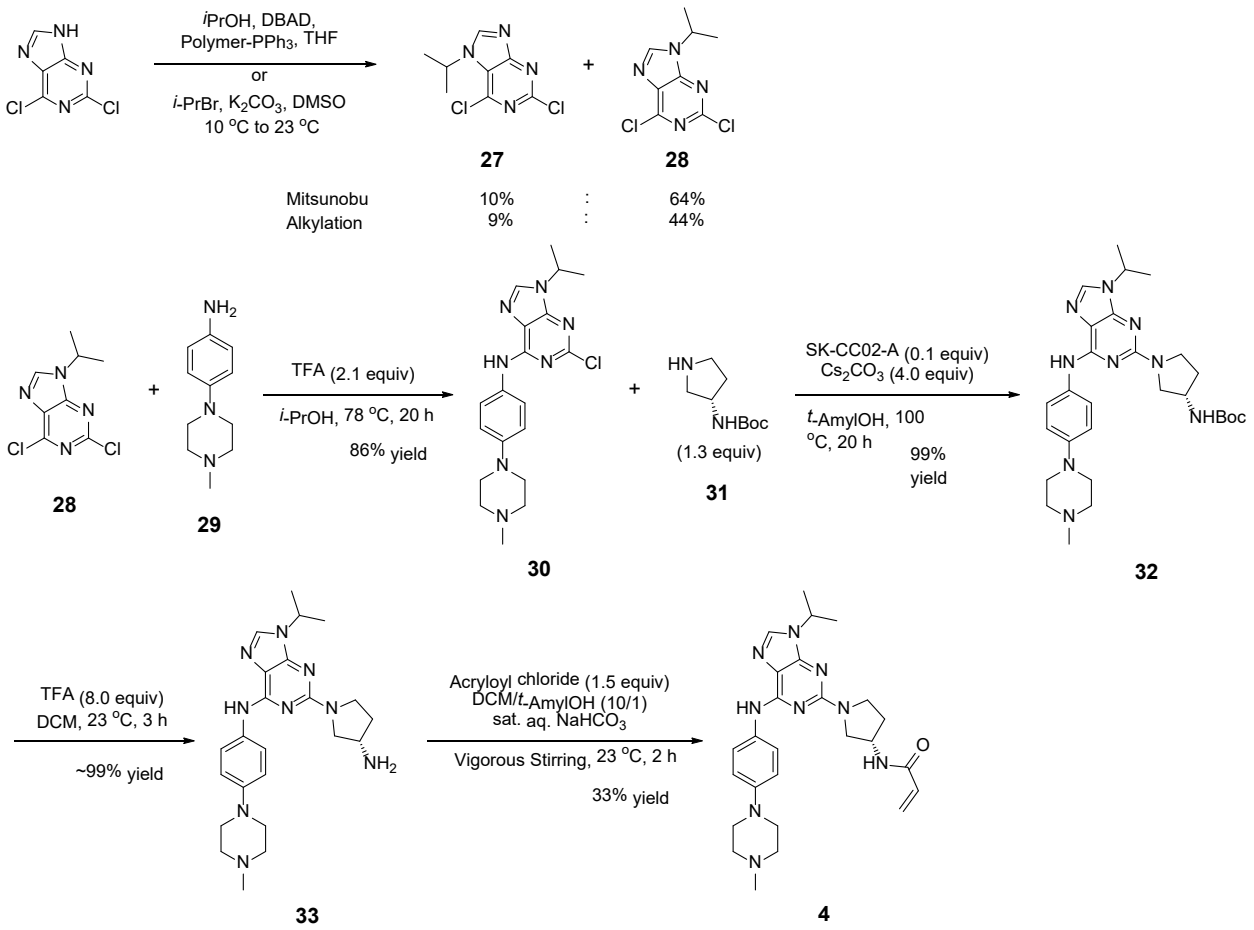

Scheme 1: Initial route exemplified by the synthesis of compound **4**.

The challenges encountered during our initial synthetic efforts led us to optimize the route to provide quicker and more robust access to diverse analogs (Scheme **2**). Specifically, our goals were to eliminate the demanding palladium-catalyzed coupling, and to improve the acrylamide formation. To obviate the need for palladium-catalyzed amination at C(2), a 2-fluoro substituent was utilized, which provided increased electrophilicity. The incorporation of a β-sulfone containing propionate fragment in pyrrolidine **36** both increased convergency and provided a masked acrylamide group that was well-behaved in amide formation. These two innovations made possible the telescoped 3-step 1-pot synthesis shown. The 2-fluoro substituent engendered sufficient electrophilicity in the system to allow sequential S_NAr reactions, but retained sufficient difference in the C(2) and C(6) reactivity to allow for complete positional fidelity in the reactions. Subsequent addition of potassium *tert*-butoxide revealed the desired acrylamide **5** in good yield.

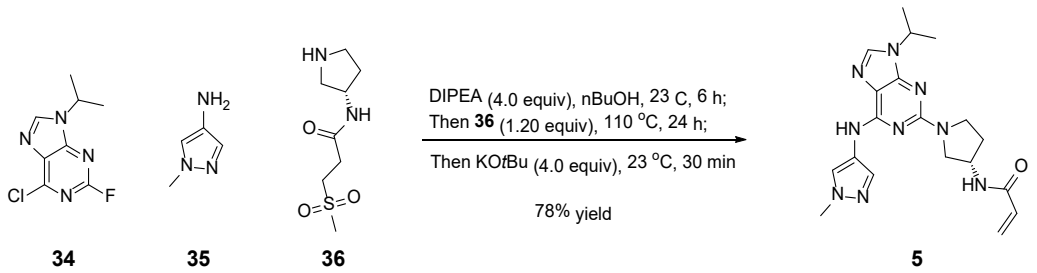

Scheme 2: Optimized analoging route exemplified by the synthesis of compound **5**.

Further refinements focused on improving the scalability of the route to compound **21** (Scheme **3**). The challenge of selective N(9) alkylation was overcome by first introducing the C(6) amine substituent and then alkylating the aminopurine intermediate. In the case of pyrazole substituted purine **39**, no N(7) alkylation could be detected. Thus, 2-fluoro purine derivative **40** underwent

S_NAr displacement with pyrrolidine **41** in high yield. Treatment of sulfone **42** with potassium *tert*-butoxide revealed acrylamide **21**. This route was executed without any chromatographic purification steps and was robust enough to produce a 100 g batch of clinical candidate **21** in support of exploratory toxicology studies.

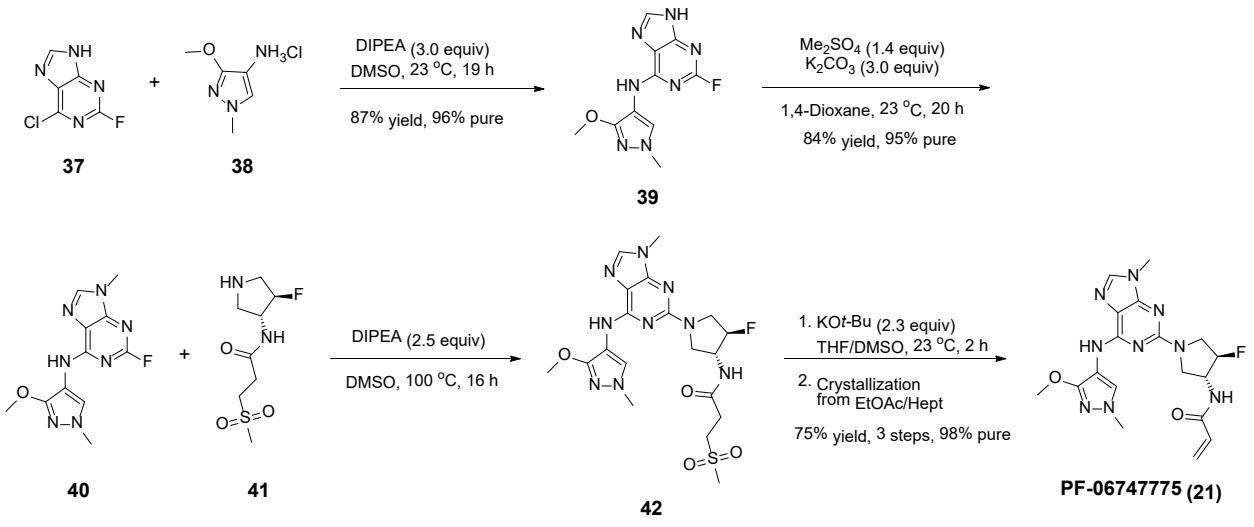

Scheme 3: Scalable route to purine compounds exemplified by clinical candidate **21**.

Conclusion: Development of a series of irreversible purine inhibitors from an initial screening hit to clinical candidate has been described. The medicinal chemistry program focused on deriving potency from *binding affinity* rather than the inactivation rate of covalent modification. This approach culminated in the discovery of **21**, a compound possessing low intrinsic reactivity, which in-turn provided reduced off-target labelling when compared to other known clinical T790M inhibitors in a cellular context. **21** has potency against both common T790M EGFR double mutants and the single point activating mutants Del and L858R whilst retaining selectivity over EGFR wild-type in order to mitigate the side effects seen with generation two EGFR irreversible inhibitors. **21** possesses an optimal balance of potency in combination with good ADME, kinase selectivity, *in vitro* and *in vivo* tox profiles. **21** has progressed into human

clinical studies as an EGFR_T790M inhibitor for NSCLC. Further details of *in vivo* efficacy, PK/PD and early clinical readouts will be published in due course.

EXPERIMENTAL SECTION

General. Starting materials and reagents were purchased from commercial suppliers and were used without further purification unless otherwise indicated. **23**, **24**, and dacomitinib were synthesized *via* Pfizer Worldwide Research and Development (La Jolla, CA, USA) using published methods. Erlotinib was purchased from LC Laboratories® (Woburn, MA, USA). All reactions were performed under a positive pressure of nitrogen or argon or with a drying tube at ambient temperature (unless otherwise stated) in anhydrous solvents (unless otherwise indicated). Reactions were assayed by high-performance liquid chromatography (HPLC) or thin-layer chromatography (TLC) and terminated as judged by the consumption of starting material. Analytical thin-layer chromatography was performed on glass-backed silica gel 60_F 254 plates (Analtech (0.25 mm)) and eluted with the appropriate solvent ratios (v/v). TLC plates were visualized by UV fluorescence, phosphomolybdic acid stain, anisaldehyde stain or iodine stain. Microwave-assisted reactions were run in a Biotage initiator. ^{1}H NMR spectra were recorded on a Bruker instrument operating at 400 MHz unless otherwise indicated. ^{1}H NMR spectra are obtained as DMSO-d6 or $CDCl_3$ solutions as indicated (reported in parts per million) using chloroform as the reference standard (7.27 ppm) or DMSO-d6 (2.50 ppm) at 30 °C unless otherwise noted. ^{13}C NMR spectra are referenced internally to solvent. ^{19}F spectra are externally referenced to $CFCl_3$ (0.0 ppm). Other NMR solvents were used as needed. When peak multiplicities are reported, the following abbreviations are used: s = singlet, d = doublet, t =

triplet, q = quartet, quin. = quintet, m = multiplet, br = broad, dd = doublet of doublets, dt = doublet of triplets. Coupling constants, when given, are reported in hertz. Mass spectra were obtained using liquid chromatography−mass spectrometry (LC−MS) on an Agilent 1260 LC with MSD Agilent model 6120 single-quadrupole mass spec detectors using atmospheric pressure chemical ionization (APCI) or electrospray ionization (ESI). High-resolution mass measurements were carried out on an Agilent TOF 6200 series with ESI. All test compounds showed >95% purity as determined by combustion analysis or by HPLC. HPLC conditions were as follows: WatersAcquityBEH C18, 2.1x30mm, 1.7µm particle size, 5-95 %B in 2.5 min, 95%B 2.5-3.0 min; Flow rate 1.2 mL/min (Solvent A: Water (0.1% formic acid + 0.05% ammonium formate) and Solvent B: Acetonitrile (5% H_2O + 0.1% formic acid + 0.05% ammonium formate)); UV detection (λ = 254, 224 nm). Combustion analyses were performed by Atlantic Microlab, Inc. (Norcross, GA).

Synthesis of 21:

2-Fluoro-*N*-(3-methoxy-1-methyl-1*H*-pyrazol-4-yl)-9*H*-purin-6-amine (39). A suspension of 6-chloro-2-fluoro-9*H*-purine (5.49 g, 31.8 mmol, 1.00 equiv), 3-methoxy-1-methyl-1*H*-pyrazol-4-amine hydrochloride (6.60 g, 40.34 mmol, 1.26 equiv), and *N*,*N*-diisopropylethylamine (16.6 ml, 95.5 mmol, 3.00 equiv) in DMSO (31.8 mL) was stirred at ambient temperature for 19 h. The reaction mixture was concentrated under reduced pressure at 50 °C, poured into water (250 mL), and stirred vigorously at 0 °C for 1 h. The resulting solids were filtered off, washed with ice cold water (20 mL), and dried for 16 h at 50 °C to give the title compound (**39**) (7.26 g, 87% yield, 96% purity) as a light yellow solid. ^{1}H NMR (400 MHz, DMSO-d_6) δ ppm 13.03 (br. s., 1H), 9.21 (br. s., 1H), 8.18 (br. s., 1H), 7.74 (br. s., 1H), 3.81 (br. s., 3H), 3.71 (s, 3H). ^{19}F NMR (377 MHz, DMSO-d_6) δ ppm -51.53 (br. s., 1F). *m/z* (APCI+) for $C_{10}H_{11}FN_7O$ 264.2 $(M+H)^+$.

2-Fluoro-*N*-(3-methoxy-1-methyl-1*H*-pyrazol-4-yl)-9-methyl-9*H*-purin-6-amine (40). To a vigorously stirred suspension of 2-fluoro-*N*-(3-methoxy-1-methyl-1*H*-pyrazol-4-yl)-9*H*-purin-6-amine (7.25 g, 27.5 mmol, 1.00 equiv) and potassium carbonate (7.61 g, 55.1 mmol, 2.00 equiv) in 1,4-dioxane (92.0 mL) was added dimethyl sulfate (2.90 mL, 30.3 mmol, 1.10 equiv) in a dropwise manner over 3 minutes. After 4 h, additional portions of 1,4-dioxane (50.0 ml), potassium carbonate (3.80 g, 27.5 mmol, 1.00 equiv), and dimethyl sulfate (1.00 mL, 10.4 mmol, 0.30 equiv) were added to the reaction mixture. After a further 16 h, the reaction mixture was concentrated under reduced pressure, diluted with water (120 mL), and stirred at ambient temperature for 1 h. The resulting solids were filtered, washed with water (20 mL), and dried at 60 °C for 16 h to give the title compound (**40**) (6.42 g, 84% yield, >95% purity) as a light yellow solid. ^{1}H NMR (400 MHz, DMSO-d_6) δ ppm 9.23 (br. s., 1H), 8.13 (br. s., 1H), 7.67 (s, 1H), 3.78 (s, 3H), 3.70 (s, 3H), 3.69 (br. s., 3H). ^{19}F NMR (377 MHz, DMSO-d_6) δ ppm -51.25 (br. s., 1F). *m/z* (APCI+) for $C_{11}H_{13}FN_7O$ 278.2 $(M+H)^+$.

***N*-((3*R*,4*R*)-4-Fluoro-1-(6-((3-methoxy-1-methyl-1*H*-pyrazol-4-yl)amino)-9-methyl-9*H*-purin-2-yl)pyrrolidin-3-yl)acrylamide (21).** To a stirred suspension of 2-fluoro-*N*-(3-methoxy-1-methyl-1*H*-pyrazol-4-yl)-9-methyl-9*H*-purin-6-amine (554 mg, 2.00 mmol, 1.00 equiv) and *N*-((3*R*,4*R*)-4-fluoropyrrolidin-3-yl)-3-(methylsulfonyl)propanamide (500 mg, 2.10 mmol, 1.05 equiv) in DMSO (4.2 mL) was added *N*,*N*-diisopropylethylamine (0.83 mL, 5.00 mmol, 2.50 equiv). The reaction mixture was heated at 100 °C for 16 h, cooled to ambient temperature, diluted with THF (4 mL), and treated with potassium *tert*-butoxide (4.00 mL, 1 M in THF, 2.00 equiv). After 1 h, an additional portion of potassium *tert*-butoxide (0.50 mL, 1 M in THF, 0.25 equiv) was added to the reaction mixture. After a further 1 h, the reaction mixture was poured into phosphate buffer (50 mL, pH 7) and water (50 mL), and extracted with ethyl acetate (5 x 40

mL). The combined organic layers were combined, dried (Na_2SO_4), and concentrated under reduced pressure. This crude product was dissolved in ethyl acetate (40 mL) at 60 °C and treated with heptanes (20 mL), at which point the solution became cloudy and was allowed to cool to ambient temperature and cooled to 0 °C. After 16 h at 0 °C, the resulting solids were filtered and dried at ambient temperature to give the title compound (**21**) (620.5 mg, 75% yield, 98% purity) as a white powder. ^{1}H NMR (400 MHz, DMSO-d_6) δ ppm 8.44 (d, *J*=6.5 Hz, 1H), 7.97 (s, 1H), 7.82 (s, 1H), 7.78 (s, 1H), 6.23 (dd, *J*=10.0, 17.0 Hz, 1H), 6.14 (dd, *J*=2.8, 17.0 Hz, 1H), 5.62 (dd, *J*=2.8, 10.0 Hz, 1H), 5.12 (d, *J* =51.0 Hz, 1H), 4.46 (td, *J*=6.0, 11.9 Hz, 1H), 3.88-3.6 (m, 4H), 3.82 (s, 3H), 3.71 (s, 3H), 3.62 (s, 3H). ^{13}C NMR (101 MHz, DMSO-d6) δ ppm 164.6, 157.3, 154.8 (br. s., 1C), 151.7 (br. s., 1C), 151.6 (br. s., 1C), 138.7, 131.1, 125.9, 125.5 (br. s., 1C), 113.2, 105.4, 94.3 (d, $J_{C\text{-}F}$=179.0 Hz, 1C), 55.9, 53.1 (d, $J_{C\text{-}F}$=29.0 Hz, 1C), 51.0 (d, $J_{C\text{-}F}$=21.0 Hz, 1C), 49.6 (br. s., 1C), 38.7, 28.9. ^{19}F NMR (376 MHz, DMSO-d_6) δ ppm -177.76 (br. s., 1F). *m/z* (APCI+) for $C_{18}H_{23}FN_9O_2$ 416.3 $(M+H)^+$. [α]D_{22}= +41.1° (c=0.5 EtOH). Calc'd for $C_{18}H_{23}FN_9O_2$ C, 52.04; H, 5.34; N, 30.34; Found: C, 52.20; H, 5.32, N, 30.46. mp 260 °C.

Biochemical Kinase Assays. EGFR kinase activity assays were reported previously[1, 27].

Cell Lines and Culture Conditions. H1975 and A549 cancer cell lines were purchased from ATCC and were cultured according to ATCC recommendations. PC9 cells were purchased from RIKEN Cell Bank (Tsukuba, Ibaraki Prefecture, Japan) and were cultured in Gibco RPMI 1640 (Life Technologies, Carlsbad, CA, USA) medium with 10% FBS (Sigma, St. Louis, MO, USA). H3255 cells were from Dr. Bruce E. Johnson at the National Cancer Institute (Bethesda, MD, USA) and were cultured in RPMI 1640, 10% FBS, and ACL-4 supplement (Mediatech Inc, Manassas, VA, USA). PC9-DRH, harboring both the single-mutant (Del) and double-mutant (Del/T790M) alleles, is a pool of cells derived from PC9 parental line that was selected after

treatment with gradually increasing concentrations of dacomitinib up to 2 μM. PC9-DRH EGFR alleles consist of 70% Del/T790M and 30% Del. PC9-DRH cells were cultured in Gibco RPMI 1640 medium with 10% FBS, and maintained in dacomitinib (2 μM).

EGFR Cellular Autophosphorylation ELISA. Cells were plated (25,000 - 50,000 cells/well) in a final volume of 100 μL of complete media in 96-well microtiter plates and cultured overnight (37 °C, 5% CO_2). Inhibitors were solubilized in DMSO and tested in duplicate utilizing 11-point serial dilutions with the highest concentration at 1 or 10 μM (0.3% v/v final DMSO). Inhibitors were incubated with cells for 2 h at 37 °C, 5% CO_2. For EGFR wild type assays, cells were plated in full-serum (10%) media for 24 h prior to compound treatment; cells were treated in full serum media as described and then stimulated for 10 min with EGF (Life Technologies) in serum-free media (50 ng/mL for A549). For all cells post inhibitor treatment (+/- EGF), media was removed and 100 μL of ice-cold lysis buffer was added: 1x cell lysis buffer (Cell Signaling Technology, Danvers, MA, USA), 1 mM phenylmethanesulfonyl fluoride (Calbiochem/EMD Chemicals, Billerica, MA, USA), 1 mM sodium orthovanadate (New England Biolabs Inc, Ipswich, MA, USA), complete Mini EDTA-free Protease Inhibitor Cocktail Tablets (Roche Applied Science, Indianapolis, IN, USA), and PhosSTOP (Roche Applied Science). Plates were shaken (20-30 min, 4 °C) to lyse the cells and 100 μL lysate was added to an ELISA plate. PathScan Phospho-EGF Receptor (Try1068) Sandwich ELISA (Cell Signaling Technology) was used to quantify EGFR autophosphorylation per the manufacturer's protocol. IC_{50} values were determined by nonlinear regression analysis with a four-parameter fit by utilizing a Microsoft Excel-based macro.

Intrinsic Chemical Reactivity Assay. The intrinsic chemical reactivity was accessed by evaluating the rate of electrophilic attack of the test compound to a strong nucleophile,

glutathione (GSH). This was achieved by monitoring test compound loss during the reaction via LC-MS/MS detection. The experiment was initiated with an aliquot (100 µL) of the test compound to a reaction buffer consisting of 100 µM phosphate buffer pH 7.4, in the presence or absence of 5mM GSH. The reaction which did not contain GSH was used as a control for chemical instability. Each compound was tested experimentally in duplicate. The final test compound concentration was 1 µM. The 37°C reaction temperature was maintained throughout the entire experiment. Aliquots of the reaction volume (100 µL) were taken at 0, 5, 15, 30, 45, 60, 90, and 120 min and quenched 1:1(v:v) with 40 mM N-ethylmaleimide (NEM) in acetonitrile containing internal standard. CI-1033 was served as the positive control in all experiments.

A linear regression analysis using the natural log of the peak area ratio, based on the internal standard, versus time provided the elimination constant (k_{el}). Half-life was calculated as ln2/ -(k_{el}). The intrinsic reactivity of each test compound was reported as the ratio of the compound half-life compared to the half-life of canertinib.

Computational Calculations: Conformation search was performed using mixed torsional/low-mode sampling method in MacroModel (Schrodinger Inc). Conformations with energies less than 5 kcal/mol relative energy were clustered, and representative conformations of each cluster were used as initial structures for the ab initio calculations. Geometry optimization was carried out at the B3LYP/6-31G(d,p) level using Jaguar (Schrodinger Inc.) v8.0. The lowest ab initio energy minima were used to calculate the relative ab initio energy for each geometry-optimized conformation.

Co-Crystal Visualizations and Protein-Ligand Modeling Methods: Pfizer in-house software was used for visualization and modeling studies. Authors will release the atomic coordinates and

experimental data upon article publication. PDB codes used in main article: 5HG7, 5UG8, 5UG9, 5UGA, 5UGB. 5UGC (for *21* as shown in TOC graphic).

In vivo work: All studies involving animals was performed in accordance with institutional guidelines as defined by Institutional Animal Care and Use Committee for U.S. institutions.

ASSOCIATED CONTENT

Supporting Information: The following is in the Supporting Information section: Focused kinase activity data for select compounds within, full kinase profiling for **21**, off-target *in vitro* assessment of **21** in a safety panel, EGFR kinetic parameters for **21**, small molecule X-ray data for **21**, proteomic compound probes (their key activity and physiochemical data and commassie gels), **21** metabolite ID and profiling, details of ADME assays, synthetic experimental details and molecular formula strings for key compounds contained within. This material is available free of charge *via* the Internet at http://pubs/acs/org.

AUTHOR INFORMTAION:

Corresponding Authors

*Email: simon.planken@pfizer.com. Phone: 858-526-4831.

*Email: douglas.behenna@pfizer.com. Phone: 858- 526-4921.

Notes: The authors declare no competing financial interest.

ACKNOWLEDGEMENTS: We are grateful to Patrick Bingham and Dawn Nowlin for HTS screening, Jun Li Feng and Kevin Ryan for protein production, Klaus Dress for data management and visualization help, Jeff Elleraas and Loanne Chung for synthetic purification work, and Greg

Stevens for pre-clinical safety discussions and considerations. Also, thanks to Dan Widlicka, Brian Samas and Alex Yanovsky for small molecule X-ray generation.

ABBREVIATIONS USED:

ADME, absorption-distribution-metabolism-excretion; EGFR, epidermal growth factor receptor; WT, wild-type; DM, double mutant (L858R/T790M, or Del/T790M); TM, triple mutant (L858R/T790M/V948R); Del, exon 19 E746-A750 deletion oncogenic mutation; SAR, structure-activity–relationships; SBDD, structure based drug design; LUMO, lowest unoccupied molecular orbital; NSCLC, non-small-cell lung cancer; TKI, tyrosine kinase inhibitor; GSH, glutathione; PK, pharmacokinetics; hLM, human liver microsome; hHEP, human hepatocytes; DOF, Dofetilide; sol, solubility; PSA, polar surface area; RRCK, permeability measured with low-efflux MDCKII cell; LipE, lipophilic efficiency; TDI, time dependent inactivation.

ADDITIONAL NOTE:

Compound **21** (catalog # PZ0302) and compound **1** (catalog # PZ0296) are commercially available *via* MilliporeSigma

REFERENCES:

1. Cheng, H.; Nair, S. K.; Murray, B. W.; Almaden, C.; Bailey, S.; Baxi, S.; Behenna, D.; Cho-Schultz, S.; Dalvie, D.; Dinh, D. M.; Edwards, M. P.; Feng, J. L.; Ferre, R. A.; Gajiwala, K. S.; Hemkens, M. D.; Jackson-Fisher, A.; Jalaie, M.; Johnson, T. O.; Kania, R. S.; Kephart, S.; Lafontaine, J.; Lunney, B.; Liu, K. K.; Liu, Z.; Matthews, J.; Nagata, A.; Niessen, S.; Ornelas, M. A.; Orr, S. T.; Pairish, M.; Planken, S.; Ren, S.; Richter, D.; Ryan, K.; Sach, N.; Shen, H.; Smeal, T.; Solowiej, J.; Sutton, S.; Tran, K.; Tseng, E.; Vernier, W.; Walls, M.; Wang, S.; Weinrich, S. L.; Xin, S.; Xu, H.; Yin, M. J.; Zientek, M.; Zhou, R.; Kath, J. C. Discovery of 1-{(3*R*,4*R*)-3-[({5-Chloro-2-[(1-methyl-1*H*-pyrazol-4-yl)amino]-

7H-pyrrolo[2,3-d]pyrimidin-4-yl}oxy)methyl]-4-methoxypyrrolidin-1-yl}prop-2-en-1-one (PF-06459988), a potent, WT sparing, irreversible inhibitor of T790M-containing EGFR mutants. *J. Med. Chem.* **2016,** *59* (5), 2005-2024.

2. (a) Sharma, S. V.; Bell, D. W.; Settleman, J.; Haber, D. A. Epidermal growth factor receptor mutations in lung cancer. *Nat. Rev. Cancer* **2007,** *7* (3), 169-181; (b) Bonanno, L.; Jirillo, A.; Favaretto, A. Mechanisms of acquired resistance to epidermal growth factor receptor tyrosine kinase inhibitors and new therapeutic perspectives in non small cell lung cancer. *Curr. Drug Targets* **2011,** *12* (6), 922-933; (c) Ohashi, K.; Maruvka, Y. E.; Michor, F.; Pao, W. Epidermal growth factor receptor tyrosine kinase inhibitor-resistant disease. *J. Clin. Oncol.* **2013,** *31* (8), 1070-1080; (d) Chang, S. C.; Chang, C. Y.; Shih, J. Y. The role of epidermal growth factor receptor mutations and epidermal growth factor receptor-tyrosine kinase inhibitors in the treatment of lung cancer. *Cancers (Basel)* **2011,** *3* (2), 2667-2678.

3. (a) Kim, Y.; Ko, J.; Cui, Z.; Abolhoda, A.; Ahn, J. S.; Ou, S. H.; Ahn, M. J.; Park, K. The EGFR T790M mutation in acquired resistance to an irreversible second-generation EGFR inhibitor. *Mol. Cancer Ther.* **2012,** *11* (3), 784-791; (b) Wheeler, D. L.; Dunn, E. F.; Harari, P. M. Understanding resistance to EGFR inhibitors-impact on future treatment strategies. *Nat. Rev. Clin. Oncol.* **2010,** *7* (9), 493-507.

4. (a) Eck, M. J.; Yun, C. H., Structural and mechanistic underpinnings of the differential drug sensitivity of EGFR mutations in non-small cell lung cancer. *Biochim. Biophys. Acta* **2010,** *1804* (3), 559-566; (b) Singh, J.; Petter, R. C.; Baillie, T. A.; Whitty, A. The resurgence of covalent drugs. *Nat. Rev. Drug Discovery* **2011,** *10* (4), 307-317; (c) Singh, J.; Petter, R. C.; Kluge, A. F. Targeted covalent drugs of the kinase family. *Curr. Opin. Chem. Biol.* **2010,** *14* (4), 475-480; (d) Yu, H. A.; Riely, G. J. Second-generation epidermal growth factor receptor tyrosine kinase inhibitors in lung cancers. *J. Natl. Compr. Canc. Netw.* **2013**, *11*, 161-169.

5. (a) Engelman, J. A.; Zejnullahu, K.; Gale, C. M.; Lifshits, E.; Gonzales, A. J.; Shimamura, T.; Zhao, F.; Vincent, P. W.; Naumov, G. N.; Bradner, J. E.; Althaus, I. W.; Gandhi, L.; Shapiro, G. I.; Nelson, J. M.; Heymach, J. V.; Meyerson, M.; Wong, K. K.; Janne, P. A. PF-00299804, an irreversible pan-ERBB inhibitor, is effective in lung cancer models with EGFR and ERBB2 mutations that are

resistant to gefitinib. *Cancer Res.* **2007,** *67* (24), 11924-11932; (b) Smaill, J. B.; Gonzales, A. J.; Spicer, J. A.; Lee, H.; Reed, J. E.; Sexton, K.; Althaus, I. W.; Zhu, T.; Black, S. L.; Blaser, A.; Denny, W. A.; Ellis, P. A.; Fakhoury, S.; Harvey, P. J.; Hook, K.; McCarthy, F. O.; Palmer, B. D.; Rivault, F.; Schlosser, K.; Ellis, T.; Thompson, A. M.; Trachet, E.; Winters, R. T.; Tecle, H.; Bridges, A. Tyrosine kinase inhibitors. 20. Optimization of substituted quinazoline and pyrido[3,4-*d*]pyrimidine derivatives as orally active, irreversible inhibitors of the epidermal growth factor receptor family. *J. Med. Chem.* **2016,** *59* (17), 8103-8124.

6. (a) Lelais, G.; Epple, R.; Marsilje, T. H.; Long, Y. O.; McNeill, M.; Chen, B.; Lu, W.; Anumolu, J.; Badiger, S.; Bursulaya, B.; DiDonato, M.; Fong, R.; Juarez, J.; Li, J.; Manuia, M.; Mason, D. E.; Gordon, P.; Groessl, T.; Johnson, K.; Jia, Y.; Kasibhatla, S.; Li, C.; Isbell, J.; Spraggon, G.; Bender, S.; Michellys, P. Y., Discovery of (*R*,*E*)-N-(7-Chloro-1-(1-[4-(dimethylamino)but-2-enoyl]azepan-3-yl)-1*H*-benzo[*d*]imid azol-2-yl)-2-methylisonicotinamide (EGF816), a novel, potent, and WT sparing covalent inhibitor of oncogenic (L858R, ex19del) and resistant (T790M) EGFR mutants for the treatment of EGFR mutant non-small-cell lung cancers. *J. Med. Chem.* **2016,** *59* (14), 6671-6689; (b) Chang, S.; Zhang, L.; Xu, S.; Luo, J.; Lu, X.; Zhang, Z.; Xu, T.; Liu, Y.; Tu, Z.; Xu, Y.; Ren, X.; Geng, M.; Ding, J.; Pei, D.; Ding, K. Design, synthesis, and biological evaluation of novel conformationally constrained inhibitors targeting epidermal growth factor receptor threonine(790) --> methionine(790) mutant. *J. Med. Chem.* **2012,** *55* (6), 2711-2723; (c) Sogabe, S.; Kawakita, Y.; Igaki, S.; Iwata, H.; Miki, H.; Cary, D. R.; Takagi, T.; Takagi, S.; Ohta, Y.; Ishikawa, T. Structure-based approach for the discovery of pyrrolo[3,2-*d*]pyrimidine-based EGFR T790M/L858R mutant inhibitors. *ACS Med. Chem. Lett.* **2013,** *4* (2), 201-205; (d) Zhou, W.; Ercan, D.; Chen, L.; Yun, C. H.; Li, D.; Capelletti, M.; Cortot, A. B.; Chirieac, L.; Iacob, R. E.; Padera, R.; Engen, J. R.; Wong, K. K.; Eck, M. J.; Gray, N. S.; Janne, P. A. Novel mutant-selective EGFR kinase inhibitors against EGFR T790M. *Nature* **2009,** *462* (7276), 1070-1074; (e) Zhou, W.; Ercan, D.; Janne, P. A.; Gray, N. S. Discovery of selective irreversible inhibitors for EGFR-T790M. *Bioorg. Med. Chem. Lett.* **2011,** *21* (2), 638-643; (f) Finlay, M. R.; Anderton, M.; Ashton, S.; Ballard, P.; Bethel, P. A.; Box, M. R.; Bradbury, R. H.; Brown, S. J.; Butterworth, S.; Campbell, A.; Chorley, C.;

Colclough, N.; Cross, D. A.; Currie, G. S.; Grist, M.; Hassall, L.; Hill, G. B.; James, D.; James, M.; Kemmitt, P.; Klinowska, T.; Lamont, G.; Lamont, S. G.; Martin, N.; McFarland, H. L.; Mellor, M. J.; Orme, J. P.; Perkins, D.; Perkins, P.; Richmond, G.; Smith, P.; Ward, R. A.; Waring, M. J.; Whittaker, D.; Wells, S.; Wrigley, G. L. Discovery of a potent and selective EGFR inhibitor (AZD9291) of both sensitizing and T790M resistance mutations that spares the wild type form of the receptor. *J. Med. Chem.* **2014,** *57* (20), 8249-8267; (g) Walter, A. O.; Sjin, R. T.; Haringsma, H. J.; Ohashi, K.; Sun, J.; Lee, K.; Dubrovskiy, A.; Labenski, M.; Zhu, Z.; Wang, Z.; Sheets, M.; St Martin, T.; Karp, R.; van Kalken, D.; Chaturvedi, P.; Niu, D.; Nacht, M.; Petter, R. C.; Westlin, W.; Lin, K.; Jaw-Tsai, S.; Raponi, M.; Van Dyke, T.; Etter, J.; Weaver, Z.; Pao, W.; Singh, J.; Simmons, A. D.; Harding, T. C.; Allen, A. Discovery of a mutant-selective covalent inhibitor of EGFR that overcomes T790M-mediated resistance in NSCLC. *Cancer Discovery* **2013,** *3* (12), 1404-1415.

7. Barf, T.; Kaptein, A. Irreversible protein kinase inhibitors: balancing the benefits and risks. *J. Med. Chem.* **2012,** *55* (14), 6243-6262.

8. Mah, R.; Thomas, J. R.; Shafer, C. M. Drug discovery considerations in the development of covalent inhibitors. *Bioorg. Med. Chem. Lett.* **2014,** *24* (1), 33-39.

9 For a discussion of a purine-derived reversible EGFR inhibitor, see: Yang, J.; Wang, L.-J.; Liu, J.-J.; Zhong, L.; Zheng, R.-L.; Xu, Y.; Ji, P.; Zhang, C.-H.; Wang, W.-J.; Lin, X.-D.; Li, L.-L.; Wie, Y.-Q.; Yang, S.-Y. Structural optimization and structure–activity relationships of N^2-(4-(4-Methylpiperazin-1-yl)phenyl)-N^8-phenyl-9*H*-purine-2,8-diamine derivatives, a new class of reversible kinase inhibitors targeting both EGFR-activating and resistance mutations. *J. Med. Chem.* **2012**, *55* (23), 10685−10699.

10. Schwartz, P. A.; Kuzmic, P.; Solowiej, J.; Bergqvist, S.; Bolanos, B.; Almaden, C.; Nagata, A.; Ryan, K.; Feng, J.; Dalvie, D.; Kath, J. C.; Xu, M.; Wani, R.; Murray, B. W. Covalent EGFR inhibitor analysis reveals importance of reversible interactions to potency and mechanisms of drug resistance. *Proc. Natl. Acad. Sci. U.S.A.* **2014,** *111* (1), 173-178.

11. Kalguthar, A. S. Should the incorporation of structural alerts be restricted in drug design? An analysis of structure-toxicity trends with aniline-based drugs. *Curr. Med. Chem.* **2015,** *22* (4), 438-464.

12. Edwards, M. P.; Price, D. A. Role of physiochemical properties and ligand lipophilicity efficiency in addressing drug safety risks. *Annu. Rep. Med. Chem.* **2010,** *45*, 380-391.

13. Krenske, E. H.; Petter, R. C.; Zhu, Z.; Houk, K. N. Transition states and energetics of nucleophilic additions of thiols to substituted alpha,beta-unsaturated ketones: substituent effects involve enone stabilization, product branching, and solvation. *J. Org. Chem.* **2011,** *76* (12), 5074-5081.

14. (a) Hunter, L. The C-F bond as a conformational tool in organic and biological chemistry. *Beilstein J. Org. Chem.* **2010,** *6,* No. 38. doi: 10.3762/bjoc.6.38; (b) Rablen, P. R.; Hoffmann, R. W.; Hrovat, D. A.; Borden, W. T. Is hyperconjugation responsible for the gauche effect in 1-fluoropropane and other 2-substituted-1-fluoroethanes? *J. Chem. Soc., Perkin Trans. 2* **1999**, 1719-1726; (c) O'Hagan, D. Understanding organofluorine chemistry. An introduction to the C-F bond. *Chem. Rev.* **2008,** *37*, 308-319.

15. Gajiwala, K. S.; Feng, J.; Ferre, R.; Ryan, K.; Brodsky, O.; Weinrich, S.; Kath, J. C.; Stewart, A. Insights into the aberrant activity of mutant EGFR kinase domain and drug recognition. *Structure* **2013,** *21* (2), 209-219.

16. (a) Bissantz, C.; Kuhn, B.; Stahl, M. A medicinal chemist's guide to molecular interactions. *J. Med. Chem.* **2010,** *53* (14), 5061-5084; (b) Zhou, P.; Zou, J.; Tian, F.; Shang, Z. Fluorine bonding--how does it work in protein-ligand interactions? *J. Chem. Inf. Model.* **2009,** *49* (10), 2344-2355.

17. Ryckmans, T.; Edwards, M. P.; Horne, V. A.; Correia, A. M.; Owen, D. R.; Thompson, L. R.; Tran, I.; Tutt, M. F.; Young, T. Rapid assessment of a novel series of selective CB(2) agonists using parallel synthesis protocols: A lipophilic efficiency (LipE) analysis. *Bioorg. Med. Chem. Lett.* **2009,** *19* (15), 4406-4409.

18. Johnson, T. W.; Richardson, P. F.; Bailey, S.; Brooun, A.; Burke, B. J.; Collins, M. R.; Cui, J. J.; Deal, J. G.; Deng, Y. L.; Dinh, D.; Engstrom, L. D.; He, M.; Hoffman, J.; Hoffman, R. L.; Huang, Q.; Kania, R. S.; Kath, J. C.; Lam, H.; Lam, J. L.; Le, P. T.; Lingardo, L.; Liu, W.; McTigue, M.; Palmer, C. L.; Sach, N. W.; Smeal, T.; Smith, G. L.; Stewart, A. E.; Timofeevski, S.; Zhu, H.; Zhu, J.; Zou, H. Y.; Edwards, M. P. Discovery of (10*R*)-7-amino-12-fluoro-2,10,16-trimethyl-15-oxo-10,15,16,17-tetrahydro-

2*H*-8,4-(m etheno)pyrazolo[4,3-*h*][2,5,11]-benzoxadiazacyclotetradecine-3-carbonitrile (PF-06463922), a macrocyclic inhibitor of anaplastic lymphoma kinase (ALK) and c-ros oncogene 1 (ROS1) with preclinical brain exposure and broad-spectrum potency against ALK-resistant mutations. *J. Med. Chem.* **2014,** *57* (11), 4720-4744.

19. Innocenti, P.; Woodward, H. L.; Solanki, S.; Naud, S.; Westwood, I. M.; Cronin, N.; Hayes, A.; Roberts, J.; Henley, A. T.; Baker, R.; Faisal, A.; Mak, G. W.; Box, G.; Valenti, M.; De Haven Brandon, A.; O'Fee, L.; Saville, H.; Schmitt, J.; Matijssen, B.; Burke, R.; van Montfort, R. L.; Raynaud, F. I.; Eccles, S. A.; Linardopoulos, S.; Blagg, J.; Hoelder, S. Rapid discovery of pyrido[3,4-*d*]pyrimidine inhibitors of monopolar spindle kinase 1 (MPS1) using a structure-based hybridization approach. *J. Med. Chem.* **2016,** *59* (8), 3671-3688.

20. (a) Greshock, T. J.; Sanders, J. M.; Drolet, R. E.; Rajapakse, H. A.; Chang, R. K.; Kim, B.; Rada, V. L.; Tiscia, H. E.; Su, H.; Lai, M. T.; Sur, S. M.; Sanchez, R. I.; Bilodeau, M. T.; Renger, J. J.; Kern, J. T.; McCauley, J. A. Potent, selective and orally bioavailable leucine-rich repeat kinase 2 (LRRK2) inhibitors. *Bioorg. Med. Chem. Lett.* **2016,** *26* (11), 2631-2635; (b) Estrada, A. A.; Chan, B. K.; Baker-Glenn, C.; Beresford, A.; Burdick, D. J.; Chambers, M.; Chen, H.; Dominguez, S. L.; Dotson, J.; Drummond, J.; Flagella, M.; Fuji, R.; Gill, A.; Halladay, J.; Harris, S. F.; Heffron, T. P.; Kleinheinz, T.; Lee, D. W.; Le Pichon, C. E.; Liu, X.; Lyssikatos, J. P.; Medhurst, A. D.; Moffat, J. G.; Nash, K.; Scearce-Levie, K.; Sheng, Z.; Shore, D. G.; Wong, S.; Zhang, S.; Zhang, X.; Zhu, H.; Sweeney, Z. K. Discovery of highly potent, selective, and brain-penetrant aminopyrazole leucine-rich repeat kinase 2 (LRRK2) small molecule inhibitors. *J. Med. Chem.* **2014,** *57* (3), 921-936.

21. (a) Di, L.; Whitney-Pickett, C.; Umland, J. P.; Zhang, H.; Zhang, X.; Gebhard, D. F.; Lai, Y.; Federico, J. J., 3rd; Davidson, R. E.; Smith, R.; Reyner, E. L.; Lee, C.; Feng, B.; Rotter, C.; Varma, M. V.; Kempshall, S.; Fenner, K.; El-Kattan, A. F.; Liston, T. E.; Troutman, M. D. Development of a new permeability assay using low-efflux MDCKII cells. *J. Pharm. Sci.* **2011,** *100* (11), 4974-4985; (b) Varma, M. V.; Gardner, I.; Steyn, S. J.; Nkansah, P.; Rotter, C. J.; Whitney-Pickett, C.; Zhang, H.; Di, L.; Cram, M.; Fenner, K. S.; El-Kattan, A. F. pH-Dependent solubility and permeability criteria for provisional

biopharmaceutics classification (BCS and BDDCS) in early drug discovery. *Mol. Pharmaceutics* **2012,** *9* (5), 1199-1212.

22. Douglas C. Behenna; Hengmiao Cheng; Sujin Cho-Schultz; Theodore O. Johnson; John C. Kath; Asako Nagata; Sajik K. Nair; Simon Planken, Purine derivatives, *Pfizer Patent* US 2015/0141402.

23. Perez-Soler, R. The role of erlotinib (Tarceva, OSI 774) in the treatment of non-small cell lung cancer. *Clin. Canc. Res.* **2004,** *10* (12 Pt 2), 4238s-4240s.

24. Lanning, B. R.; Whitby, L. R.; Dix, M. M.; Douhan, J.; Gilbert, A. M.; Hett, E. C.; Johnson, T. O.; Joslyn, C.; Kath, J. C.; Niessen, S.; Roberts, L. R.; Schnute, M. E.; Wang, C.; Hulce, J. J.; Wei, B.; Whiteley, L. O.; Hayward, M. M.; Cravatt, B. F. A road map to evaluate the proteome-wide selectivity of covalent kinase inhibitors. *Nat. Chem. Biol.* **2014,** *10* (9), 760-767.

25. Eaton, D. L.; Bammler, T. K. Consise review of the glutathione S-transferases and their significance to toxicology. *Toxicol. Sci.* **1999,** *49*, 156-164.

26. Gintant, G. An evaluation of hERG current assay performance: Translating preclinical safety studies to clinical QT prolongation. *Pharmacol. Ther.* **2011,** *129* (2), 109-119.

27. Schwartz, P. A.; Kuzmic, P.; Solowiej, J.; Bergqvist, S.; Bolanos, B.; Almaden, C.; Nagata, A.; Ryan, K.; Feng, J.; Dalvie, D.; Kath, J. C.; Xu, M.; Wani, R.; Murray, B. W. Covalent EGFR inhibitor analysis reveals importance of reversible interactions to potency and mechanisms of drug resistance. *Proc. Natl. Acad. Sci. U.S.A.* **2014,** *111* (1), 173-178.

TOC GRAPHIC

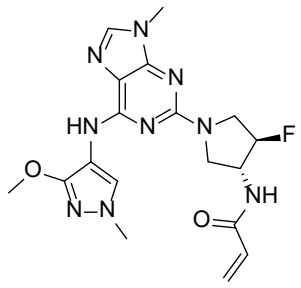

21

EGFR L858R_T790M IC_{50} 12 nM
EGFR Del_T790M IC_{50} 3 nM
EGFR L858R IC_{50} 4 nM
EGFR Del IC_{50} 5 nM
EGFR WT IC_{50} 307 nM